DEPOSITIONAL MODELING AND INTERACTION BETWEEN LITHOFACIES

ASSEMBLAGES OF CRETACEOUS-PALEOGENE STRATA OF THE RATON

BASIN

by

Sean Corbett Horne

Bachelor of Science in Geology, 2016

Colorado State University

Fort Collins, CO

Submitted to the Graduate Faculty of

The College of Science and Engineering

Texas Christian University

In partial fulfillment of the requirements for the degree of

MASTER OF SCIENCE IN GEOLOGY

December 2018

Acknowledgements

I would like to thank my parents and family for their continual support throughout all my years of schooling. I would like to thank my Dad for brainstorming ideas and always encouraging me to think outside of the box. To my mom, I would like to thank her for her continued support and being a voice of reason. I would like to thank the TCU Geology Department for providing me with an opportunity to learn and grow. A special thanks to Dr. John Holbrook, my thesis advisor, for providing his guidance and expertise throughout this entire process. I would like to thank Dr. Richard Denne and Bo Henk for serving on my committee. I would also like to thank Pioneer Natural Resources for the funding provided for this project. I want to thank Ross Harrison for being an awesome partner on this project. I would also like to thank my fellow graduate students at TCU as well as my friends back home for their continued support and words of encouragement.

Table of Contents

List of Figures

List of Tables

CHAPTER ONE: Introduction

The Raton Basin of northeastern New Mexico and southeastern Colorado (Figure 1) is a prolific producer of coal bed methane. Coal from the Raton and Vermejo formations have produced over 1.5 Trillion cubic feet of gas since the beginning of production in 1982 (Osterhout, 2014). Currently there are approximately 7,000 wells within the Raton Basin. Of the 7,000 wells, 4,000 are producing natural gas from the coal bearing formations within the Raton Basin (Osterhout, 2014).
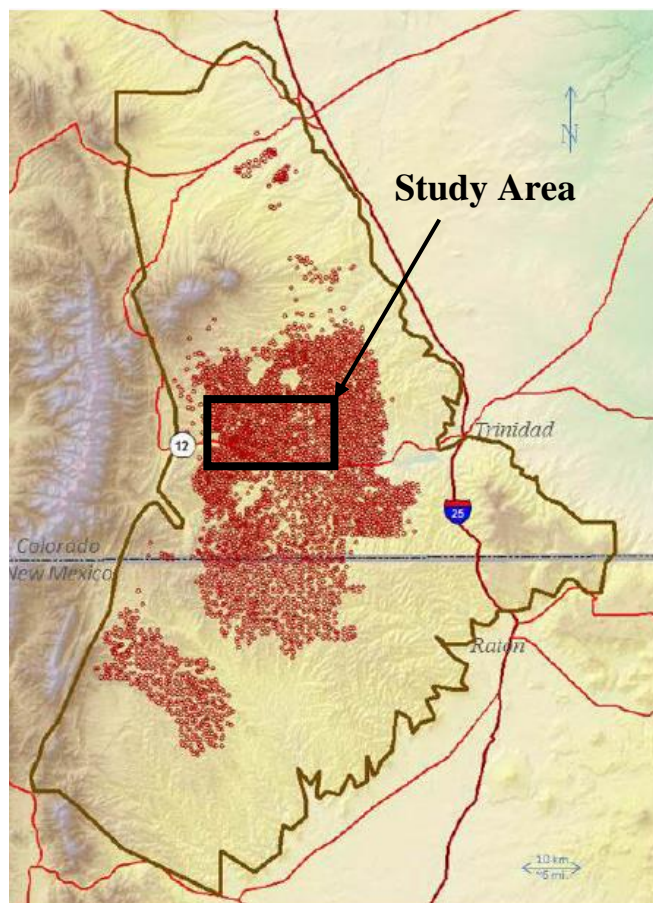
Figure 1: Locater map for the Raton Basin (outlined in brown) and study area (outlined in black). Coal bed methane wells indicated by red dots (Osterhout, 2014).

The interaction between the dryer, coal-poor and wet, coal-rich lithofacies assemblages of the Raton Formation is not fully understood. The objective of this study is to develop a better understanding of the depositional environments of the informal Raton Formation members. This work utilizes well log correlations, core descriptions, measured sections, and digital outcrop models to create paleogeographic reconstructions of the Raton Formation depositional systems. In addition, this study aims to determine the interaction between the different lithofacies assemblages. I propose that a Distributary Fluvial System deposited Raton Formation sediments. I hypothesize that the basal conglomerate and barren series of the Raton Formation were deposited in the proximal zone of a distributary fluvial system, whereas the upper and lower coal zones of the Raton Formation were deposited in the distal zone. The purpose of this study is to help determine the predictive distribution of coal bearing strata and its connectivity to the reservoir-prone, fluvial sandstones of the Raton Formation to aide in natural gas production.

Geologic Background

Raton Basin:

The Raton Basin is an elongate, asymmetric foreland basin located in northeast New Mexico and southwest Colorado (Figure 2) (Baltz, 1965; Hoffman and Brister; 2003). The Sangre de Cristo Mountains, and the Sierra Grande bound this north-south trending structural basin to the west and the Las Animas arch binds the basin to the east. The Wet Mountains bound the basin to the North, and the Cimarron Mountains to the South (Figure 2) (Johnson et al., 1956; Baltz, 1965; Flores, 1987). The basin is approximately 174 miles long, and 65 miles at its widest, spanning roughly 2,500 square miles (Johnson and Wood, 1956).
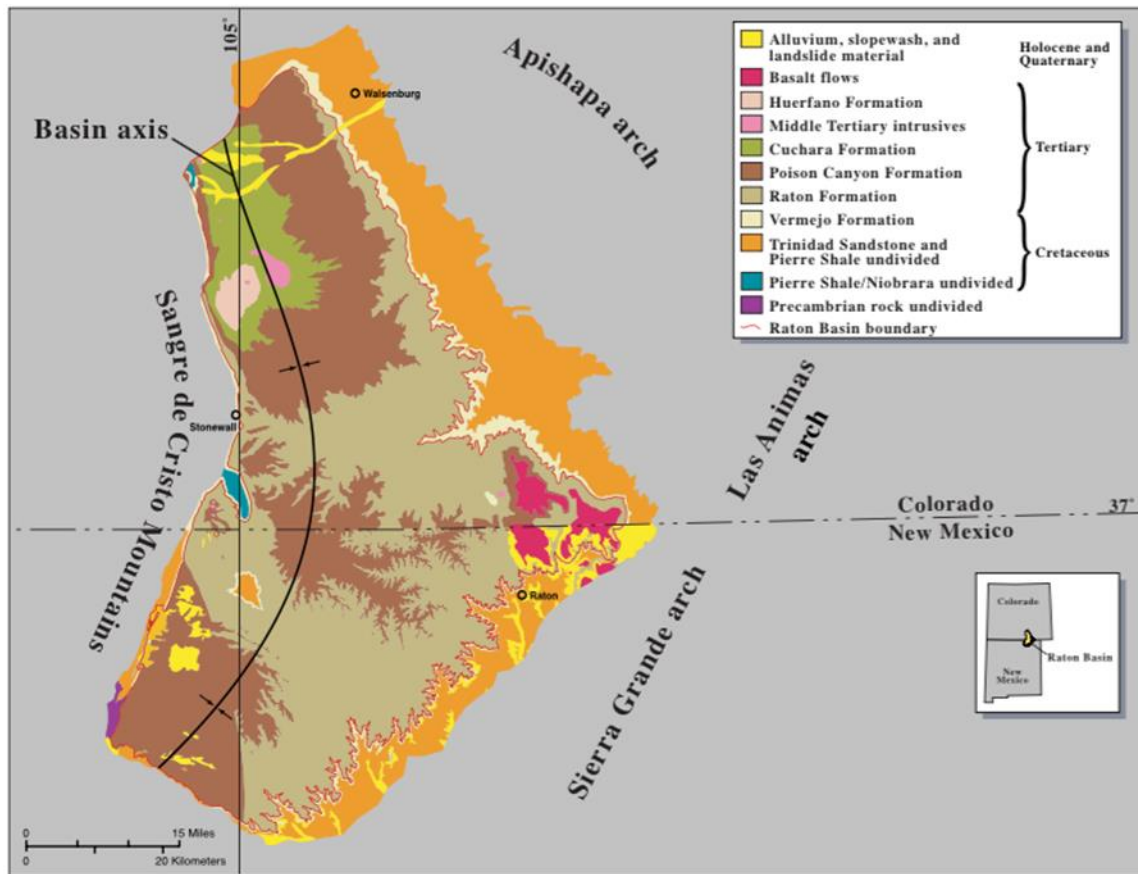
Figure 2: A geologic map of the Raton Basin displaying major structural features and stratigraphic units (Johnson and Finn, 2001).

The basin axis is located along the western basin margin and varies from north to south, slightly deviating to the northwest in Colorado and slightly southwest in New Mexico (Figure 2) (Pillmore, 1976 Johnson and Finn, 2001). Beds that define the western margin of the basinward steeply inclined and overturned by Laramide thrusting, which pushed Precambrian and Paleozoic strata over younger rock. Beds on the east side of the basin dip 1 to 5 degrees towards the west (Pillmore, 1976; Pillmore and Flores, 1987; Flores and Bader, 1999; Johnson and Finn, 2001; Clarke, 2004; Topper, 2011; Bush et al., 2016).

During early Paleozoic time, the present-day location of the Raton Basin was tectonically stable. In late Paleozoic time, uplift of the Sangre de Cristo Mountains forced development of a major depositional center within the Raton Basin (Woodward, 1983; Strum, 1985). During the late Mesozoic, the basin was part of the Western Interior foreland basin and was transformed into the current day intermontane basin during the Laramide Orogeny (Pillmore, 1976). Structural bounds of the basin were generated during periods of folding and thrusting in the Eocene and were enhanced by normal faulting in the late Cenozoic during epiorogenic upwarping (Johnson and Wood, 1956; Horner, 2016). Extrusive and intrusive volcanism occurred along the Sierra Grande Arch in the late Cenozoic times (Woodward, 1983).

Late Cretaceous and Tertiary Stratigraphy

Upper Cretaceous stratigraphy of the Raton Basin comprises both marine and non-marine sediments. The marine Pierre Shale (Campanian to Maastrichtian) underlies the marginal marine Trinidad Sandstone. Non-marine sedimentary rocks of the Raton Basin include the Vermejo Formation (Maastrichtian), Raton Formation (Maastrichtian and Paleocene), and Poison Canyon Formation (Maastrichtian and Paleocene) (Pillmore and Mayberry, 1976; Billingsley, 1977; Pillmore and Flores 1990).

The Pierre Shale (Figure 3) is a dark, silty non-calcareous shale. (Pillmore and Flores, 1990). This 1,800 to 1,900 ft. thick, shale was deposited in prodeltaic and offshore marine environments of the Cretaceous Western Interior Seaway (Figure 4) (Johnson et al., 1956). The shale grades upward into the Trinidad Sandstone through a Maastrichtian-aged transition zone that comprises interbedded shale, siltstone, and sandstones containing *Ophiomorpha* burrows (Pillmore and Flores, 1987; Johnson and Finn, 2001). The overlying Trinidad Sandstone (Figure 3) ranges from 0 to 300 feet in thickness throughout the western margin of the basin. It is composed

of very fine- to fine-grained sandstone containing trace fossils of the *Skolithos* ichnofacies, including *Ophiomorpha, Diplocraterion* (Pillmore and Flores, 1990). The Trinidad Sandstone was deposited in delta-front and shoreline environments during the eastward progradation of the Cretaceous coastline (Figure 4) (Pillmore and Flores, 1987; 1990). To the west, the Raton Formation locally truncates the Trinidad Sandstone, but elsewhere the Trinidad is overlain by the Vermejo Formation (Pillmore and Flores, 1990)

AGE		FORMATION NAME	GENERAL DESCRIPTION	LITH-OLOGY	APPROX. THICKNESS IN FEET
TERTIARY	PALEOCENE	POISON CANYON FORMATION	SANDSTONE–Coarse to conglomeratic beds 13–50 feet thick. Interbeds of soft, yellow-weathering clayey sandstone. Thickens to the west at expense of underlying Raton Formation		500+
		RATON FORMATION	Formation intertongues with Poison Canyon Formation to the west UPPER COAL ZONE–Very fine grained sandstone, siltstone, and mudstone with carbonaceous shale and thick coal beds BARREN SERIES–Mostly very fine to fine-grained sandstone with minor mudstone, siltstone, with carbonaceous shale and thin coal beds LOWER COAL ZONE–Same as upper coal zone; coal beds mostly thin and discontinuous. Conglomeratic sandstone at base; locally absent		0(?)–2,100 ← K/T boundary
MESOZOIC	UPPER CRETACEOUS	VERMEJO FORMATION	SANDSTONE–Fine to medium grained with mudstone, carbonaceous shale, and extensive, thick coal beds. Local sills		0–380
		TRINIDAD SANDSTONE	SANDSTONE--Fine to medium grained; contains casts of *Ophiomorpha*		0–300
		PIERRE SHALE	SHALE--Silty in upper 300 ft. Grades upward to fine-grained sandstone. Contains limestone concretions		1800-1900

Figure 3: A generalized stratigraphic column of the Raton Basin displaying Late Cretaceous and Paleocene strata (Pillmore, 1969; Flores, 1985; Flores, 1987; Pillmore and Flores, 1987; Johnson and Finn, 2001).

The Vermejo Formation (Figure 3) conformably overlies the Trinidad Sandstone in the north. The Vermejo Formation comprises interbedded sandstones, siltstones, shales, carbonaceous shales, and coal. Along the western margin of the basin, the Vermejo Formation varies from 370 feet to 390 feet in thickness and thins to 0 feet on the eastern margin of the basin (Pillmore, 1976; Pillmore and Flores, 1990). The Vermejo Formation was deposited contemporaneously with the

Trinidad Sandstone on fluvial-deltaic and back-barrier plains (Figure 4) (Pillmore and Flores, 1990)

The Raton Formation (Figure 3) ranges in thickness from 1,100 feet in the eastern portion of the basin to 2,100 feet in the western and central portions of the basin (Lee and Knowlton, 1917; Pillmore, 1969; Flores, 1987; Flores and Bader, 1999; Topper et al., 2011). Three informal members comprise the Raton Formation: the lower coal zone, the barren series, and the upper coal zone (Figure 6) (Johnson et al, 1956).
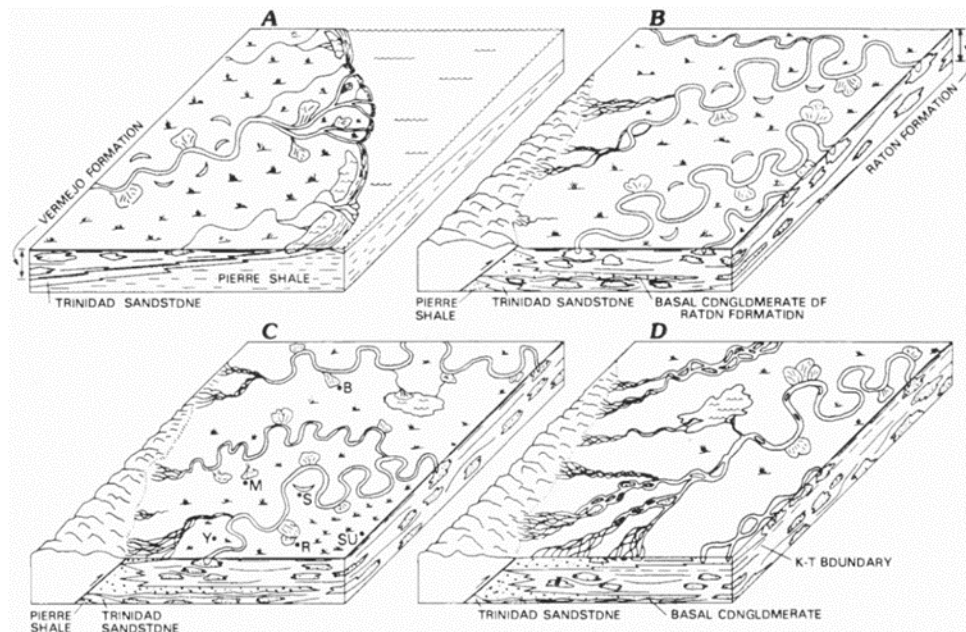
Figure 4: Block diagrams showing the development of the fluvial system and the surrounding depositional environments (A) Pierre Shale, Trinidad Sandstone, and Vermejo Formation; (B) lower coal zone of the Raton Formation; (C) the end of the lower coal zone of the Raton Formation, and (D) the barren series of the Raton Formation (Pillmore and Flores, 1987).

The Poison Canyon Formation (Figure 3) overlies the Raton Formation throughout most of the basin. However, to the west and southwest, the Poison Canyon intertongues with the Raton Formation (Figure 5) (Flores and Pillmore, 1987; Pillmore and Flores 1990). The Poison Canyon Formation varies in thickness from 0-2,500 feet. The Poison Canyon consists of interbedded

coarse-grained conglomeratic sandstones, mudstones, and siltstones (Johnson et al, 1966) and fines toward the eastern part of the basin.
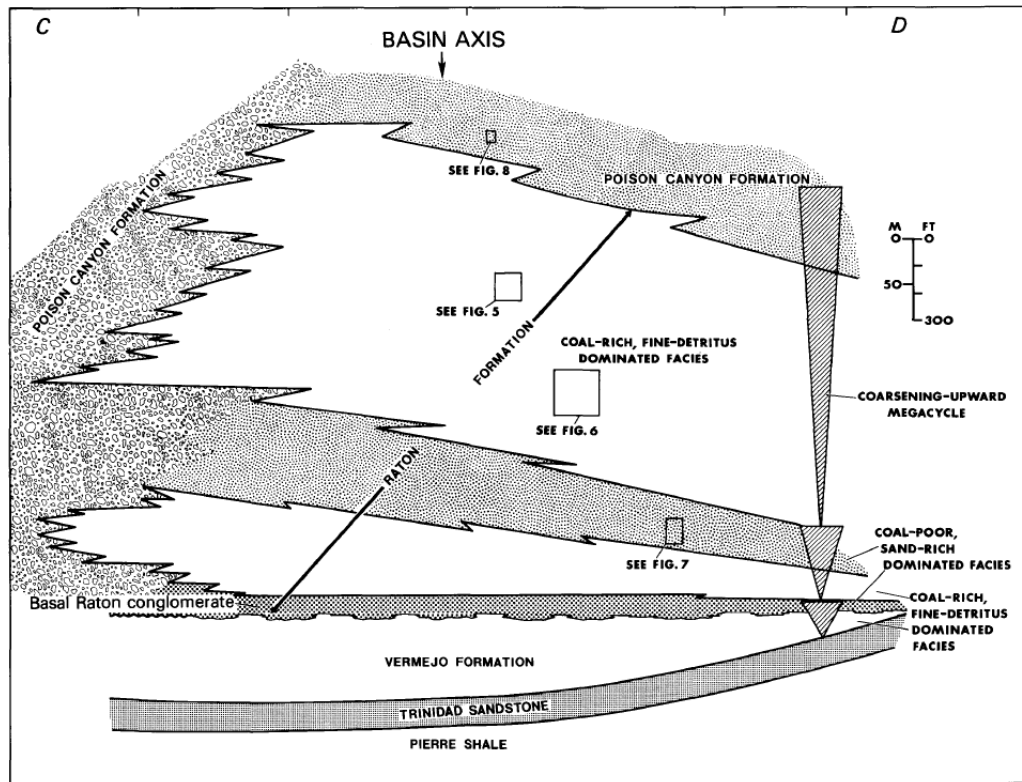
Figure 5: A generalized cross-section displaying the intertonguing relationship between the Raton and Poison Canyon formations (Flores and Pillmore, 1987).

Raton Formation

The Raton Formation was deposited on an upper alluvial plain during the end of the Late Cretaceous and into the Paleocene (Figure 4). The Raton Formation comprises three members and reaches a maximum thickness of 2,100 feet in the west-central part of the basin (Pillmore, 1976, Strum, 1985; Pillmore and Flores, 1987; Pillmore and Flores, 1990; Hoffman and Brister, 2003). The lower coal zone ranges in thickness from approximately 100 feet to 300 feet along the western margin of the basin. It is composed of siltstones, sandstones, carbonaceous shales, and coal beds, interbedded with channel belt sandstones (Pillmore and Flores, 1990). At the base of the lower

7

coal zone is a 0 to 30-foot-thick discontinuous, pebble conglomerate. The basal conglomerate is thickest in the southwestern portion of the Raton Basin and thins to the east. The pebble conglomerate fines upward to a coarse-grained sandstone and has an erosional contact with the underlying Vermejo Formation (Pillmore and Flores, 1990; Hoffman and Brister, 2003). Overlying the basal conglomerate are finer grained floodplain and coaly deposits interbedded with channel belt and levee deposits interpreted as deposits of meandering rivers (Figure 6) (Flores, 1985). The Cretaceous-Paleogene boundary is at the top of the lower coal zone and is marked by an iridium anomaly that coincides with the disappearance of Cretaceous taxa and a change from angiosperm pollen to fern spores (Pillmore and Flores, 1984; 1987; Orth et al., 1987; Flores and Bader 1999; Horner, 2016).

The barren series ranges in thickness from 200 feet to 600 feet (Hoffman and Brister, 2003). According to Flores (1985), channel derived lithofacies dominate the barren series, which thickens and coarsens to the west into sheet-like conglomerates. Coal and carbonaceous shale beds are sparse in this member of the Raton Formation. These thin, discontinuous, organic-rich deposits are interbedded with minor deposits of silty sandstones, siltstones, and mudstones, as well as channel-fill sandstone (Flores, 1985). The barren series has been interpreted as high-bedload meandering stream and braided stream deposits (Figure 6). The intertonguing conglomeratic Poison Canyon Formation is interpreted as alluvial fan deposits (Flores, 1985; Flores, 1987; Flores and Bader, 1999). Uplift and erosion of the source area during the Late Cretaceous and early Paleocene provided a pulse of conglomeratic detritus that resulted in rapid lateral migration of stream channels, which accounts for the poor preservation of floodplain environments (Woodward, 1983; Flores 1985; Flores and Bader, 1999). Wolfe and Upchurch (1987) suggested the sediment supply increase is also be attributed to the annihilation of the surrounding vegetation due to the K-Pg

extinction event subsequently changing erosional and floral patterns within the Raton Basin during the deposition of the barren series (Pillmore and Fleming, 1990; Pillmore et. al., 1999).

The upper coal zone comprises predominately fine-grained sediments and ranges in thickness from 600-1100 feet thick. (Pillmore and Flores, 1990, Johnson and Finn, 2001; Norwest Corporation, 2010). This member is dominantly siltstone and mudstone beds interbedded with channel and crevasse-splay sandstones. The unit includes laterally continuous coals up to 12 feet thick and abundant carbonaceous shales (Flores, 1985; Pillmore and Flores, 1990; Johnson and Finn, 2001). The upper coal zone deposited in poorly drained floodplains featuring crevasse splays, single or multistory channel bodies, and abandoned channel lithofacies (Figure 6) (Flores 1985; Flores and Bader, 1999). Coal layers and thick floodplain deposits of the upper coal zone record a relative shift in base level allowing for more accommodation. The creation of more accommodation is attributed to active subsidence (tectonic and/or sediment loading) throughout the basin (Flores, 1985).

Previously published studies attribute the deposition of the Raton Formation to intra- and extrabasinal tectonism. Extrabasinal tectonism of the Laramide Orogeny produced pulses of sedimentation that led to deposition of the basal conglomerate and barren series (Flores, 1987; Flores and Pillmore, 1987; Pillmore and Flores). During periods of tectonic stability, deposition of fine-grained sediments occurred leading to the formation of the upper and lower coal zones (Flores, 1987; Flores and Pillmore, 1987; Pillmore and Flores, 1990; Flores and Bader, 1999; Horner, 2016). This depositional model of the three informal members of the Raton Formation is reliant on separating and assigning different fluvial styles to each member (Pillmore, 1976). However, work done by Horner (2016) contradicts this model. Horner (2016) suggests the barren series are local expressions of sections rich in valley fill. The valley fills represent trunk channels

that incised up to 80 feet with lateral extents of 1,500 feet (Clarke et al., 2002; Norwest Corporation, 2010). The high sediment volumes accompanying deposition of the valley fill sediments would likely hinder economic peat accumulation (McCabe and Parrish, 1992; Miall, 1996; Horner, 2016).

In the context of the distributary fluvial system (DFS) model, the Raton Formation was deposited in the distal zone of the DFS fan (Horner, 2016). The units bearing thick coal and carbonaceous shales beds record the most distal portions of the fan at times where the spring line is at or near the surface. This increase in accommodation favors the accumulation of peat (Diessel, 1992; Bohacs and Suter, 1997). Valley fill sediments, channel belts, terminal splays, and crevasse splays reflect upland, higher energy environments, which account for the higher abundance of net sand (Hartley et al, 2010; Horner, 2016.)
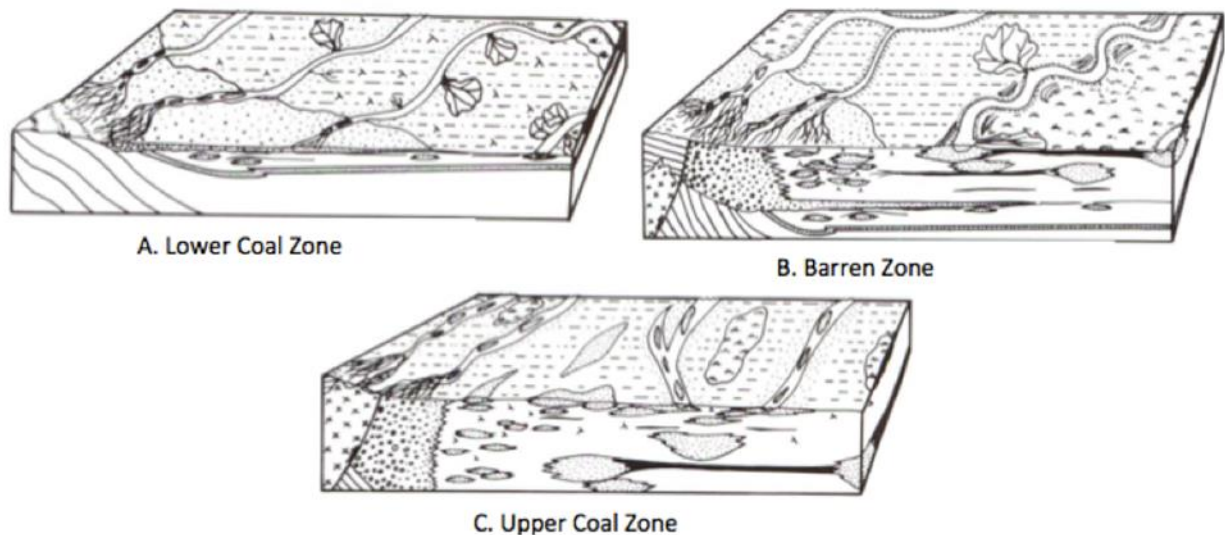
Figure 6: Block diagram displaying the different depositional environments of the lower coal zone, barren series, and upper coal zone of the Raton Formation (Flores, 1985).

Distributary Fluvial System:

A distributary fluvial system (DFS) is a river system characterized by a downstream decrease in sediment discharge, grainsize, river gradient, and channel dimensions because of a loss of water discharge caused by lateral dispersion and evaporation. (Figure 7 and 8)(Nichols and Fisher, 2007). Loss of gradient, driving a loss of channel confinement, triggers DFS systems, which are typical of subsiding basins. In the distal low-gradient zone, channel dispersion commonly occurs, forming terminal splays on either dry alluvial plains or onto lakes as deltas (Nichols and Fisher, 2007). Distributary fluvial systems commonly occur in a climate where it is warm and dry enough that there is a net water loss. (Nichols and Fisher, 2007). However, distributary fluvial systems can also form in humid environments (Hartley et al., 2010 McGregor, 2017). Hartley et al. (2010) identified 415 DFS systems globally and concluded that DFS's developed in a multitude of different climatic environments including: drylands, tropical, subtropical, continental, and polar. They also determined that this fluvial system forms in multiple tectonic settings including: extensional, compressional, strike-slip, and cratonic (Hartley et al, 2010). None of these variables fully controls the DFS formation as a large DFS can form in any climate or tectonic setting (Hartley et al, 2010).

Length of a DFS is limited by the available horizontal accommodation space, which is predominantly related to the tectonic setting of the basin (Hartley et al, 2010). Foreland basins and cratonic tectonic settings produce the largest DFSs as they contain large basinward slopes where wide lateral systems can develop. Extensional and strike-slip basins are much narrower, therefore limiting the lateral accommodation available for DFSs formation (Hartley et al, 2010).
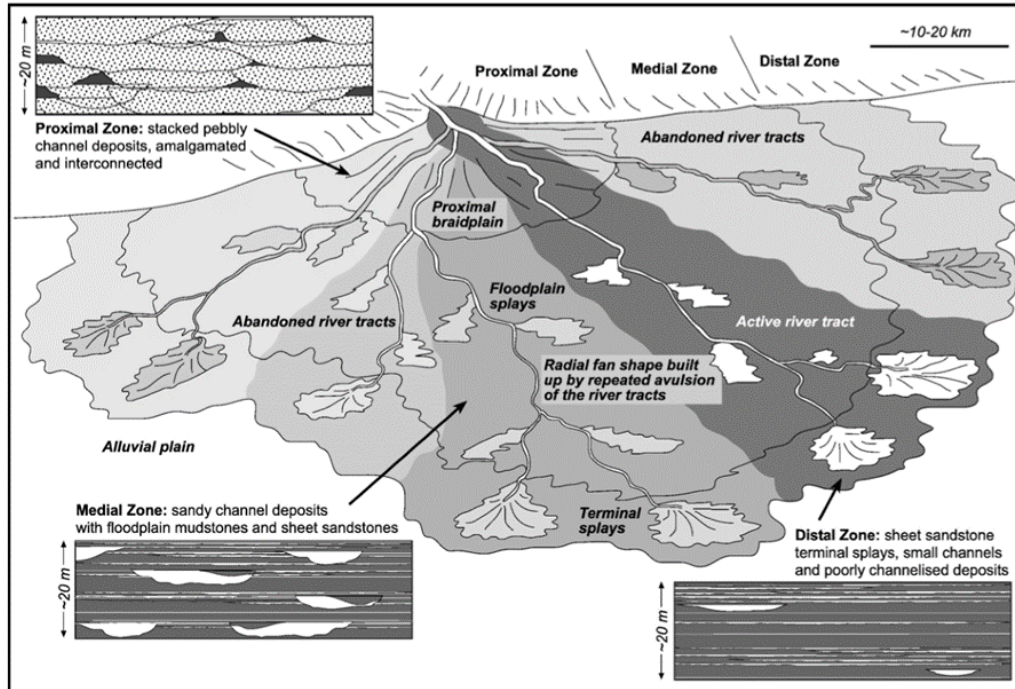
Figure 7: Depositional model of a distributary fluvial system (Nichols and Fisher, 2007)

Braided planforms typify all tectonic settings, especially compressional regimes where a high gradient is present. These high gradient braided streams are associated with areas of high relief and arid climates, where discharge is commonly more intermittent (Hartley et al, 2010). However, sinuous planforms are associated with wetter, more tropical climates and tend to have more perennial fluvial systems that can distribute bedload more efficiently (Hartley et al, 2010).
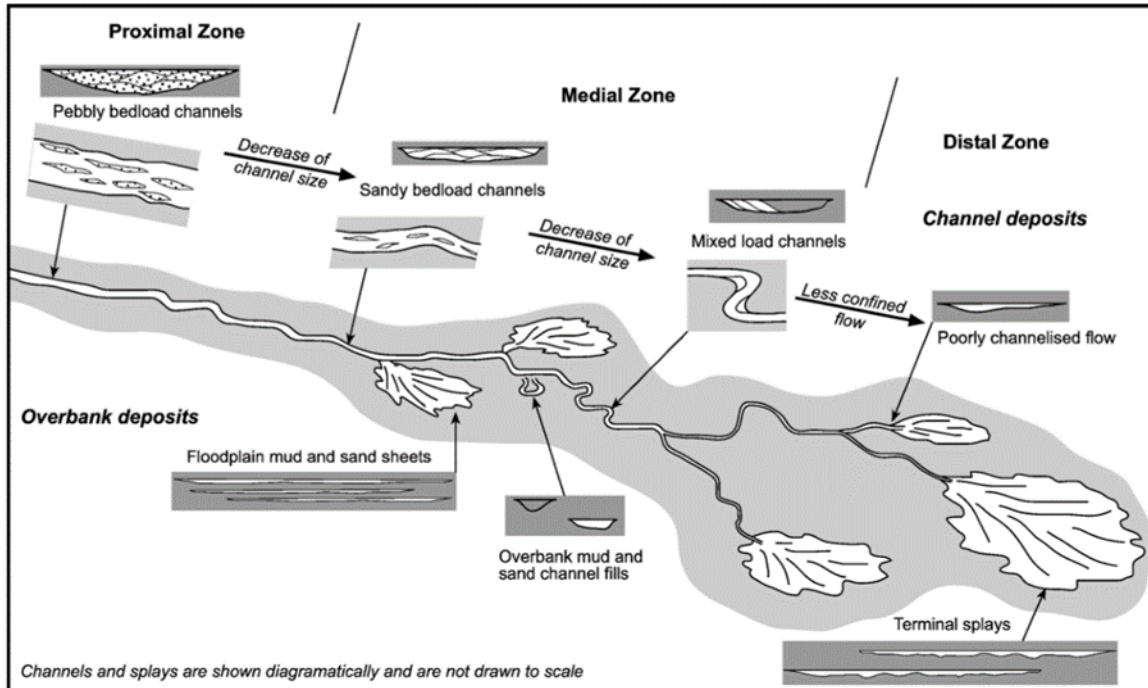
Figure 8: Diagram of a distributary fluvial system illustrating the different characteristics and features of each zone (Nichols and Fisher, 2007).

Distributary fluvial systems form a radial pattern (Figure 7), spreading out across the alluvial plain in a fan shape (Nichols and Fisher, 2007). The terms "fluvial fan" and "fluvial megafans" have also been used in the past to describe DFS systems. The term fluvial fan describes a low gradient fan, usually <0.1˚, that forms by the avulsion of channelized streams (Nichols and Fisher, 2007; Hartley et al, 2010). The term fluvial megafan delineates a difference in scale, where fluvial fans are typically miles across and megafans are tens of miles across (Nichols and Fisher, 2007; Hartley et al, 2010). These planforms are not to be confused with alluvial fans which should be reserved for describing steep, debris flow and sheetflood dominated deposits with a gradient >1˚ (Nichols and Fisher, 2007).

The three zones that comprise the DFS model include a proximal zone, a medial zone, and a distal zone (Figure 8) (Nichols and Fisher, 2007). The proximal zone is the point at which the

channels are the largest and most deeply incised (Nichols and Fisher, 2007). This zone is composed of sandy to conglomeratic facies with imbrication, cross-bedding, and preservation of bar structures close to the margin of the basin (Graham, 1983; Nichols, 1987; MacCarthy, 1990; Sadler and Kelly, 1993; Nichols and Fisher, 2007). Fine-grained overbank flow deposits are not preserved in the proximal zone as the channel-fill facies are entirely amalgamated (Nichols and Fisher, 2007). Channels migrate laterally here and repeated avulsion reworks floodplain deposits (Nichols and Fisher, 2007).

In the medial zone (Figure 8), overbank deposits, such as floodplain splays, become more prevalent (Nichols and Fisher, 2007) as channel-fill bodies become more laterally stable (MacCarthy, 1990; Hirst, 1991). Channel-fill bodies comprise finer grained sediments and are predominantly mudstones and thin sheet bodies of sandstone (Nichols and Fisher, 2007). The overbank deposits found within the medial zone may show evidence of desiccation or the formation of soil (Graham, 1983; Nichols and Fisher, 2007).

The distal zone (Figure 8) of the distributary fluvial system is predominantly floodplain facies and intermittent channel-fill deposits that are generally shallow and undefined due to unchannelized flow (Graham, 1983; Sadler and Kelly, 1993; Nichols and Fisher, 2007). Mudstones typically fill the channel scours within the distal zone suggesting localized channelization (Graham, 1983; Nichols and Fisher, 2007). Rivers that cannot maintain flow across a whole basin will terminate within the basin (Hartley et al, 2010), depositing terminal splay complexes onto the alluvial floodplain (Fisher et al, 2007). The distal zone of distributary fluvial systems has laterally extensive sheets of sandstone, thought to be terminal splays, bounded by muddy, silty units interpreted as paleosols (Sadler and Kelly, 1993; Fisher et al., 2008; Nichols and Fisher, 2007). Within the distal zone, there is a decrease in slope, channel size, infiltration, sediment load, and

evapotranspiration (Hartley et al, 2010). With the decrease in slope, the channels become less laterally mobile which promotes growth of vegetation and floodplain stabilization (Nichols and Fisher, 2007). The distal zone of the DFS system is also where coal deposition is most likely. In the distal zone, the groundwater table evaluation, or spring line, controls accommodation (Bohacs and Suter, 1997). Maximum preservation of organics occurs when the spring line is at or near surface elevation. This is because accommodation is high and vegetation that typically grows in peatland environments thrives in this ever-wet type of environment (Diessel, 1992; Bohacs and Suter, 1997; Harrison, 2018).

Coal Depositional Models

Coal beds of the Raton Formation originally were described as discrete and discontinuous beds that generally do not extend more than one thousand feet before depositional pinch out or truncation by a fluvial channel (Flores and Bader, 1999; Clarke et al., 2002; Topper, 2011; Harrison, 2018). More recent studies contradict this, suggesting coals can be mapped for miles throughout the basin (Osterhout, 2014; Harrison, 2018; Roy Pillmore, Personal Comm. 2018). The most popular coal depositional model (Flores, 1985) describes coal deposition in the abandoned floodplain of meandering rivers (Figure 5) (Flores, 1985; Harrison, 2018). This model suggests that the floodplain was situated in the distal, poorly drained portion of the flood basin, during a period of rapid subsidence. Depositional loading forced the water out of the pore space, subsequently raising the water table relative to the ground elevation, aiding in peat preservation (Flores, 1985; Harrison, 2018). More recently, Harrison (2018) argued that coals were not deposited in discrete and ephemeral swamps, but in short-lived peat-friendly phases of long lasting, extensive lake systems of a fluvio-lacustrine system.

Lithofacies:

Lithofacies were determined in core and outcrop for the upper and lower coal zones of the Raton formation by Robert Horner (2016) and Ross Harrison (2018). Robert Horner (2016) described the barren series lithofacies in outcrop. Lithofacies are a mappable subdivision of a stratigraphic formation that is distinguishable by texture and sedimentary structures. Cretaceous-Paleogene Raton Formation strata contain 13 unique lithofacies (Table 1) as determined from core and outcrop.

Grain Size	Lithofacies (Code)	Lithology	Characteristics	Fossils, Special Features	Interpretation
C	Conglomerate (Cg)	Pebble-sized, poorly sorted conglomerate, reddish brown	No major observable features, massive, poorly sorted conglomerate	None observed	Braided streams and alluvial fan deposits, upper flow regime, represents Raton Conglomerate
S	Trough cross-laminated sandstone (St)	Fine to coarse-grained quartzose sandstone , white (fresh) to dark tan / yellow (weathered)	Sets range in thickness from 0.1-2m, commonly at base of multiple sandstone sets	Commonly in scour at base, frequent mud rip-ups and local preserved organics (sticks)	Migration of dunes, high energy flow
S	Planar cross-laminated sandstone (Spx)	Fine to coarse-grained quartzose sandstone , white (fresh) to dark tan / yellow (weathered)	Sets range in thickness from 0.1 to 3.5m and tend to fine up. Scours within / between sets identifiable. Contains both low and high angle cross-laminations	Commonly in scour at base, some preserved organics (sticks)	Dunes and bars in low flow regime
S	Planar-laminated sandstone (Sp)	Very fine to coarse-grained quartzose sandstone, white (fresh) to dark tan / yellow (weathered)	1mm-1cm horizontal laminations, with lamination sets ranging from 1-75cm. Contain isolated ripple laminations	Abundant preserved organics at base (leaves, stick impressions)	Upper flow regime plane bed
S	Ripple-laminated sandstone (Sr)	Very fine to medium-grained quartzose sandstone, white (fresh) to tan (weathered)	1-3 cm ripple laminations, ripple sets ranging from 0.5-20cm, rare climbing ripples	Abundant preserved organics (leaves, sticks)	Channel, splay, and blowout wing. Represents ripple migration in low flow regime.
S	Massive sandstone (Sm)	Very fine to coarse-grained quartzose sandstone, white (fresh) to dark tan / yellow (weathered)	Lack of sedimentary structures, Thickness ranges 0.1-2m	Preserved whole trees, directly associated gravity-driven collapse structures	High volume sand movement of channel sands
M	Slumped sandstone (Sss)	Silty sandstone to medium-grained sandstone, ranges in color due to high argillaceous content	Dewatering structures common, some preservation of primary sedimentary structures but typically destroyed	None observed	Represent gravity-driven flows, bank collapse, slump structures, liquefaction

M	Faintly-laminated sandstone (Sfl)	Very fine to medium-grained quartzose sandstone, ranges in color (white-yellow-red) due to high argillaceous content	Contains faint low-angle laminations, one of the most common lithofacies	Common preserved organics (roots, leafs, sticks)	Formed during brief deceleration of high volume sand flow or Sm
M	Heterolithic Sandstone, Siltstone, Mudstone (H)	Lithology ranges from muddy siltstone to medium-grained sand, occurs in alternating bedding	planar-laminated, ripple-laminated, or faintly-laminated, Thickness ranges from 0.05-4m	Commonly rooting near top of H, but generally lacks bioturbation, some well-preserved organics in between laminations	Splay delta, waning flows, and abandoned channel fills
F	Laminated Mudstone (Flm)	Clay particles, slightly silty mudstone to pure mudstone, light to dark gray	Planar-laminations	Minor preserved organics (sticks, leafs), iron staining and nodules, some pyrite, very minor rooting	Floodplain lakes, with minor rooting and iron staining indicating temporary exposure
F	Paleosol (Fp)	Occurs in mud and siltstone to very fine-grained quartzose sandstone	Most characterized by rooting, primary bedding typically destroyed. Commonly, gleyed, mottled, containing slickenlines	Dominated by moderate to abundant rooting,	Moderately to very poorly drained, poorly developed simple soils. Slickenlines indicate vertisols, mottled and broken up / green paleosols indicate gleysol
F / O	Carbonaceous Mudstone (Fcm)	Dark gray to very black. Often shiny. Very fissile.	Often preserved, coalified organics. Abundant organics differentiate this lithofacies from laminated mudstone. Range in thickness from 0.02-1.5m	Sticks, roots, leafs, generally have been coalified	Basically coaly mudstones, and serve as a transitionary period between when floodplain lakes are not coal-producing.
O	Coal (C)	Black, shiny, high volatile bituminous a coal.	Well-developed cleats. Range in thickness from 0.03-2.5m	Shiny, black	Period during which floodplain lakes undergo period of peat-preservation

Table 1: Table of lithofacies identified in core and outcrop by Harrison (2018) and Horner (2016). Includes information on lithology, major characteristics, fossils and special features, and interpretations of each. The following denote grain size: Cg=Conglomerate, S=Sand, M=Mixed Fines and Sand, F=Fines, and O=Organics.

Lithofacies Assemblage:

Harrison (2018) and Horner (2016) grouped lithofacies identified in outcrop and core into genetically related lithofacies assemblages. They identified four major assemblages including channel-belt, lacustrine, floodplain, and terminal splay assemblages. Harrison (2018) also identified a valley-fill super-assemblage. This super-assemblage is composed of a combination of assemblages. Channels cutting through lake and floodplain deposits create the channel-belt assemblage. Lake deposits, including coals, comprise the lacustrine assemblage and the subaerial floodplain deposits make up the floodplain assemblage. Subaerial sheetflood deposits that have propagated from the terminus of a distributary channel are associated with the terminal splay lithofacies assemblage (Horner, 2016).

The upper and lower coal zones of the Raton Formation are composed of the channel-belt, floodplain, and lacustrine lithofacies assemblages. Valley-fill super-assemblages were also identified in outcrops of this unit. Horner (2016) identified multiple lithofacies assemblages and super-assemblages within the barren series, including the valley-fill super-assemblage, channel-belt, floodplain, terminal splay, and to a lesser extent lacustrine lithofacies assemblages.

<u>Channel-Belt Assemblage:</u>

The channel-belt assemblage contains Cg, St, Spx, Sp, Sr, Sm, Sss, Sfl, and Fp lithofacies (Table 1). The channel assemblage ranges from fine-grained quartzose sandstone to pebbly conglomeratic sandstones. This assemblage typically fines upwards and is generally well sorted. The channel-belt assemblage comprises three elements: bars, channel fills, and wings (Harrison, 2018). Of these elements, the channel fill is the most prevalent, followed by the bar, and the blowout wing elements. Channel-belts are commonly clustered or amalgamated.

Ross Harrison (2018) derived channel story thickness from four cores and three outcrops. Channel story thicknesses ranges in size from 0.5 m to 6.5 m, with an average thickness of 4 m. Channel stories are measured from the basal scour to an upward lithofacies change to either the lacustrine or the floodplain lithofacies.

Channel Fill Element

The Channel Fill element is composed of the Cg, St, Spx, Sr, Sm, Sss, and Sfl lithofacies (Table 1). Channel fills within the Raton Formation range in thickness from 1.5 m to 8 m and extend laterally from 1 m to 100 m (Harrison, 2018). Channel fills have a concave up, lensoid geometry. Generally, channel fills will have a basal scour, fine upwards, and are well sorted. Channel fills, like the channel-belt assemblage, are encased in either floodplain or lacustrine sediments (Harrison, 2018).

Bar Elements

Channel bars comprise lithofacies St, Sxp, Sp, and Sr (Table 1). Bars typically have lensoid or sheet-like geometries and display an erosive basal contact. Channel bars fine upwards, have internal accretion sets and a lensoid geometry (Miall, 1996; Sharma, 2013; Harrison, 2018).

Blowout Wing Element

Tomanka (2013) first described blowout wings as sand sheets deposited perpendicular to channels propagating into floodplain lakes or lacustrine environments. Blowout wing elements comprise lithofacies Sp, Sr, Sm, and Sfl (Table 1). Blowout wings generally occur at the top of channel fills and extend laterally on either side of the channel. These sand sheets are approximately .5 meters thick can extend upwards of 300 meters (Tomanka, 2013; Huling, 2014; Harrison, 2018).

Terminal Splay Lithofacies Assemblage:

The Terminal Splay Lithofacies Assemblage comprises lithofacies St, Sr, Sp, Sm, Flm, and Fp (Table 1). Individual terminal splay beds range in thickness from 0.15 meters to 1 meter, and can amalgamate into complexes up to 2.5 m thick. Individual beds can extend laterally from 20 meters to 100 meters (Horner, 2016). Terminal splays are typically ripple and planar laminated, trough cross-bedded, or massive. This lithofacies is also commonly associated with vegetation induced sedimentary structures in the form of upturned beds (Horner, 2016). The Terminal Splay lithofacies assemblages are typically well-rounded and well-sorted, fine- to medium-grained sandstones (Horner, 2016).

Floodplain Assemblage:

The floodplain lithofacies assemblage includes lithofacies Sp, Sr, H, Flm, Fcm, and C (Table 1). The floodplain lithofacies assemblage contains predominantly poorly drained floodplain elements, but also includes moderately drained elements. Coals and carbonaceous (C) mudstone are sparse within the floodplain assemblage. However, very thin, discontinuous beds of C occur within the poorly drained floodplain deposits. The floodplain assemblage ranges in thickness from 0.5 meters to 8 meters and can be very laterally extensive if not scoured or truncated by a channel.

Lacustrine Assemblage:

The lacustrine lithofacies assemblage comprises lithofacies Sr, Sfl, H, Fp, Flm, Fcm, and C (Table 1). The lacustrine lithofacies assemblage ranges in thickness from 0.5 meters to 8 meters and is typically laterally extensive when not truncated by channels. This assemblage is similar to the floodplain lithofacies assemblage, but with a higher abundance of coal, laminated mudstone, and carbonaceous mudstone. There is also far less rooting within the lacustrine assemblage

because it is deposited subaqueously. Coals within the lacustrine assemblage are much thicker and laterally extensive. Coals are typically encased in laminated and carbonaceous mudstones. Coals within the upper coal zone of the Raton Formation have been mapped over distances greater than ten miles (Osterhout, 2014; Roy Pillmore, Personal Comm. 2018; Harrison, 2018).

CHAPTER TWO: Methods and Data

To determine the distribution of coal and its connectivity to fluvial sandstones, this project utilized a wide array of subsurface data. Well log data was acquired from the Colorado Oil and Gas Conservation Commission (COGCC). Wells within the Raton Basin are typically logged using gamma ray, density, and deep induction resistivity. Using these well logs, formation tops, lithosomes, and coals were correlated throughout the study area to create isopach maps. Isoliths were calculated utilizing well log cut offs to determine the spatial distribution of the different lithologies found throughout the Raton Formations. From these maps, interpretations of the depositional environment were made.

Well Log Data:

This project utilized subsurface data to determine a depositional model for the Raton Formation. The Raton Basin is penetrated by approximately 7,300 wells on an 80-acre spacing. Of these 7,300 wells, only 3,000 of them have publicly available well logs. The log suite that is generally ran on these wells consists of a gamma ray, caliper, density porosity, neutron porosity, and a density log. The study is further limited to digital logs from the Colorado side of the Raton Basin. Logs from 1,003 wells were acquired from the COGCC using the Colorado Oil and Gas Information System (COGIS). Wells, roads, townships, and counties were uploaded to a map using the North American Datum 1927 (NAD 27) coordinate system in IHS Petra (Figure 9).
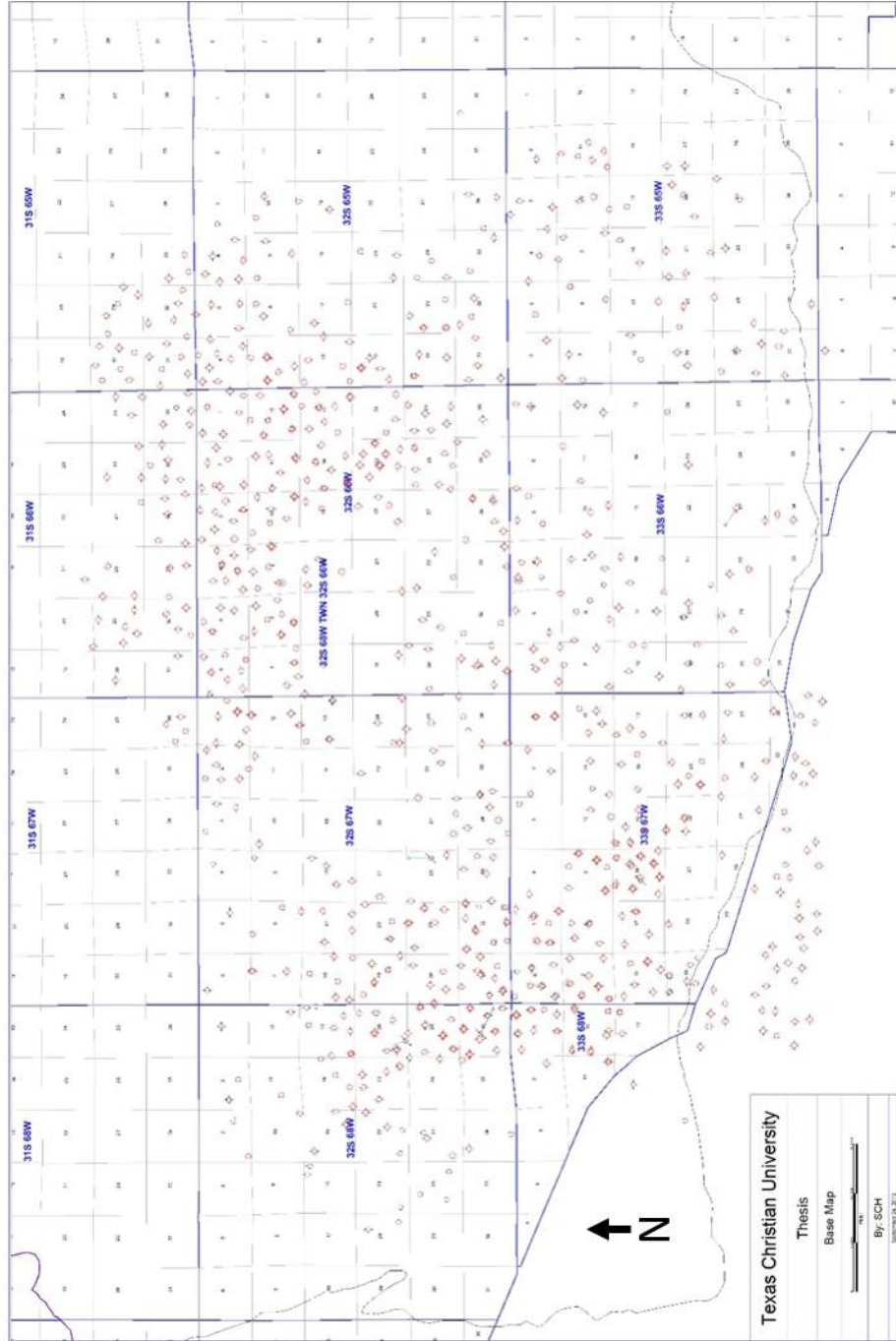
Figure 9: Base map of the study area displaying major highways, townships, sections, and coal bed methane wells.

Well Log Methods:

Digital well files were imported into Petra using a 14-digit unique well identifier (UWI). Wells were then plotted onto a map using NAD27 coordinates to determine their spatial distribution. Once wells were uploaded, major roads, townships, and counties were uploaded to the map through the "culture" tab in Petra. Following the population of the map, the digital well files including drillers reported tops, IHS tops, production data, well information (i.e., spud date, completion date, etc.), and digital logs (Figure 9) were assigned to their corresponding well utilizing their UWI.

The main logs used for this project were the gamma ray, density, and deep resistivity. The main use of the gamma ray tool is to determine lithology. The tool measures emissions from the naturally occurring radioactive materials (NORM) found within the minerals in the rock. The NORM typically include elements such as uranium, thorium, and potassium. Organic rich shales are more likely to contain these elements than sandstones. This allows for differentiation between the two lithologies in a gamma ray well log.

A density log is used to measure the density of the surrounding rock, giving the interpreter information on the lithology of the rock. The density log works by emitting electrons into the surrounding rock that are either scattered or absorbed. The tool then detects those that are scattered back. A high return of electron particles indicates a high-density rock while a low return indicates a low-density rock. Essentially, the tool is measuring the electron density of the formation and converting it into bulk density.

The deep resistivity log measures the electrical resistivity of a formation. Resistivity is measured by inducing a current into the formation and measuring the conductivity. Traditionally, resistivity is used to measure rock type, porosity, fluid type, and fluid saturations. However, within the Raton Formation, resistivity is an excellent indicator of volcanically intruded zones.

Using the three logs, lithologies were determined within the Raton Formation. A gamma ray reading of less than 100 API units and a density reading of approximately 2.65 g/cc (Figure 10) indicates the presence of sandstone in the well log. A low gamma ray reading coupled with a density below 1.5 g/cc indicates the presence of coal in the well. A high resistivity response coupled with the low gamma ray reading also indicates the presence of coal within a well. (Figure 10). Shales are identified in well logs through their high gamma ray. The shales within the Raton Formation are differentiated into the floodplain/lake and carbonaceous shales. Carbonaceous shales tend to have a lower, more erratic density reading because of high woody organic material content (Figure 10). The floodplain shales tend to have a density reading of approximately 2.7 g/cc (Figure 10). Finally, intrusions are identified by large, erratic resistivity anomalies on the well logs (Figure 10). A low gamma ray response and a higher density reading accompany these anomalies.
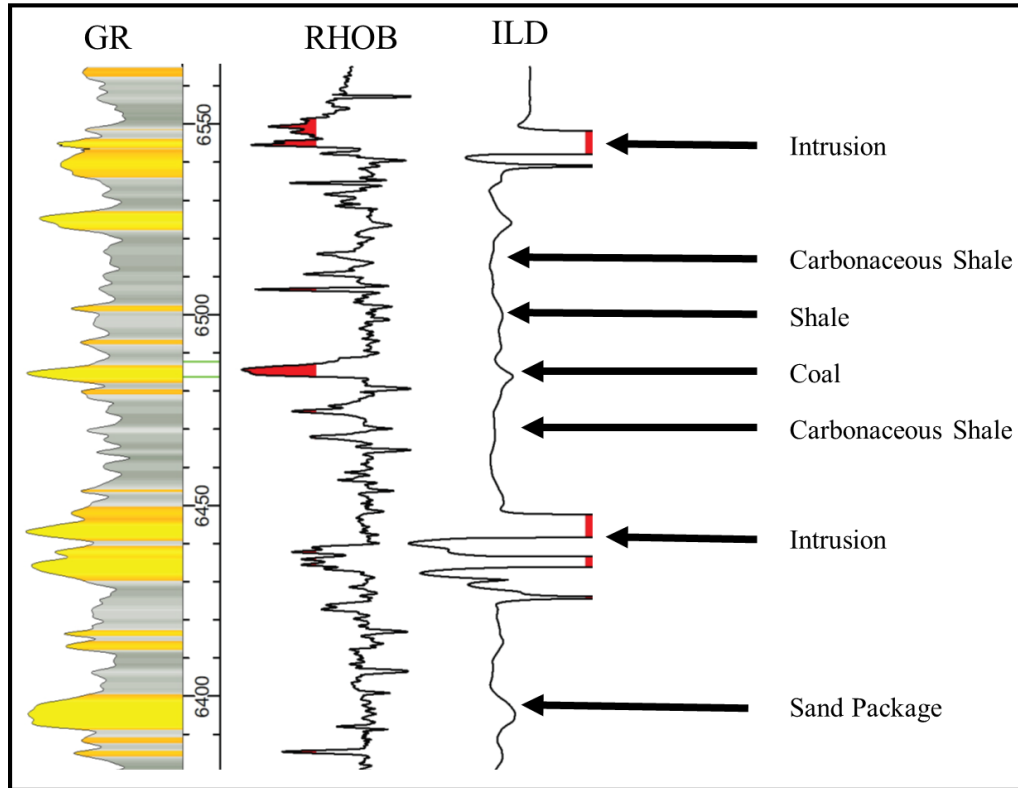
Figure 10: A well log suite from Squeal 11-26 located in township 32W60S section 26 showing log signatures for the different lithologies found within the Raton Formation

Correlation Methods:

Formation tops were correlated utilizing Petra's cross-section module. The Trinidad Sandstone pick is based on its high sandstone content and lack of coal. The occurrence of the lowermost coal indicates the base of the Vermejo Formation and the top of the Trinidad Formation. The basal Raton Conglomerate marks the top of the Vermejo Formation. In well logs, this unit appears as a very low, blocky gamma ray response. The Raton Formation top is rarely present within the study area owing to erosion (Figure 11).

The "coal x" top was correlated across the Raton Basin. The "coal x" top is determined by tying the Tru_3 coal found within the Zamora 22-14V, to the well log and correlating outward in a spiral fashion. This coal is locally intruded, indicated by an erratic deep resistivity response. This is common as coals are weaker than the surrounding rock and act as a conduit for the intrusion to expand. Once correlated, this coal was used as a stratigraphic maker and a datum.

The informal members of the Raton Formation are correlated throughout the basin utilizing outcrop and core studies (Horner, 2016; Harrison, 2018). These studies defined characteristic lithofacies and lithofacies assemblages that are used here to calibrate subsurface data. Measured sections were completed to identify key architectural elements and create detailed lithofacies models. Along Colorado Highway 12, Harrison (2018) completed architectural element analyses of fluvial deposits (Miall, 1985; 1988; Maill and Bridge; 1995) within the upper and lower coal zones of the Raton Formation. Previous work by Horner (2016) identified lithofacies models of the barren series.
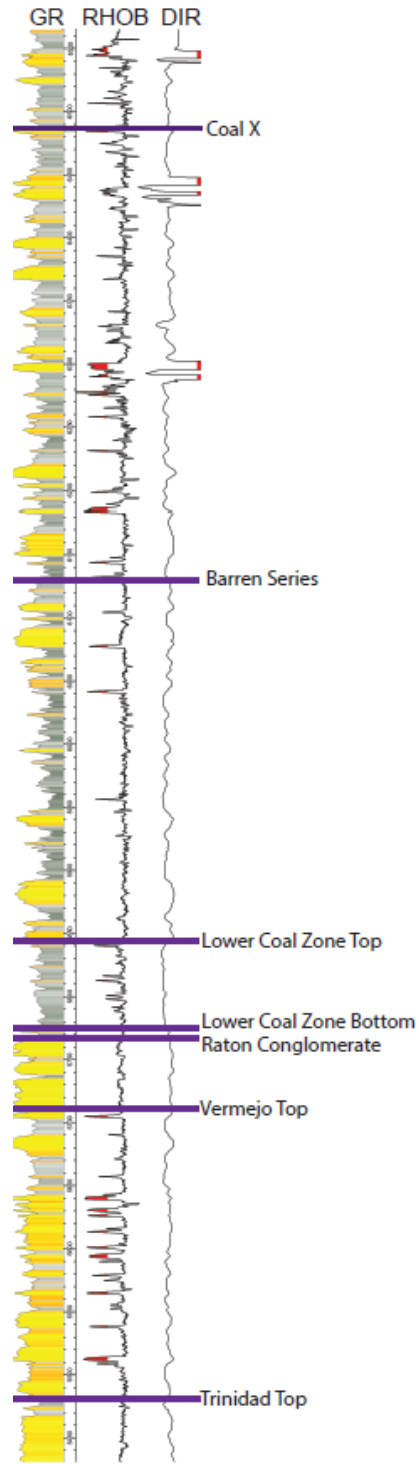
Figure 11: A well log showing the different tops throughout the Raton Formation

Mapping:

Isopach maps of the formations and informal members were generated using Petra's isopach computation tool. From these maps, cumulative interval thicknesses were made for each individual well. From those thicknesses, sandstone, mudstone, and coal thicknesses were calculated using well log cut offs and Petra's reservoir property tool. Sandstones are defined, as intervals where the API value on the gamma ray was less than 100 units combined with the density value being above 2 grams /cc. Coals are defined as intervals where the API value on the gamma ray log was less than 100 units combined with the density value being below 1.5 g/cc. Shales are defined as intervals where the API value on the gamma ray log was greater than 100 API units. From these values, sandstone, shale, and coal percentages were calculated utilizing Petra's equation expression tool and plugging in the formula below. From the values derived, isoliths were created to indicate where each lithology is concentrated throughout the study area.

$$\% \, \textbf{Rock Lithology} = \frac{\textbf{\textit{Cumulative Rock Lithology (Sand, Shale, Coal)}}}{\textbf{\textit{Formation Total Thickness}}}$$

Interval count maps were generated utilizing the "Log Footage Summation (Reservoir Properties)" and the previously mentioned cutoffs for the sandstone lithology. Footage cut offs were used as a tool to help identify the depositional environment for the different sandstone packages throughout the study area when combined with other maps. The footage cutoffs are as follows: 1 ft to 5 ft, 5ft to 10 ft, 10 ft to 15 ft, and 15 ft to 20 ft.

CHAPTER 3: Results

Cross Sections:

Cross section one (Figure 12) depicts stratigraphic relationships in the Raton Basin and includes nine wells selected across the Raton Basin from the southwest to northeast. Each well displays a gamma ray log, density log, and resistivity log. The gamma ray log is on track one. API values lower than 100 units are color filled with yellow. Values higher than 100 units are color filled with gray. The density log is on track two. The red color fill indicates values lower than 2 g/cc. The deep induction resistivity log is on the third track. The red color fill indicates values greater than 1000 ohms. The cross section is hung off the coal x datum.

The Vermejo Formation top is defined by the sharp contact between the fine-grained sediments of the Vermejo Formation and the coarser Raton conglomerate. In well logs, this contact displays as a very low gamma ray reading immediately overlying a high gamma ray reading. Coal is not found within the Raton conglomerate. Within the Vermejo Formation, coal signatures, indicated by low-density readings (RHOB), are abundant (Figure 11). The Vermejo shows a thinning trend to the northeast. The top of the Raton Conglomerate is gradational from coarser, conglomeratic sediments to finer grained sediments and coal within the lower coal zone. In well logs, this gradational change is shown by gamma ray readings becoming higher as the tool moves shallower in depth. In addition, the density reading will become more erratic as coal is present within this interval. Thicknesses of the Raton conglomerate varies along the southwest-northeast trend. The lower coal zone (LCZ) top is marked by a transitional zone between LCZ and the barren series. Within the transition zone, coal becomes less prevalent and sediments coarsen, which is shown through lower gamma ray readings and the density log remaining static at approximately 2.65g/cc. The LCZ displays a general thinning trend to the east. The barren series top is defined

31

by the return of major coals into the system and a transition from coarse-grained sediments back to finer sediments. This return of major coals within well logs is indicated by low-density anomalies in the density log. In addition, the gamma ray tends to be higher due to the increase in mudstone within the upper coal zone compared to the barren series. Overall, the barren series shows a dramatic thinning to the northeast. Coals found in the northeastern portion of the basin display a distinct onlapping relationship with the barren series interval (Figure 12). Coal x is the highest mappable coal within the study area. Harrison (2018) described this coal from the Zamora 14-22v well. The coal x to barren series interval shows a thickening to the northeast. This interval contains the distal coals that are lapping onto the barren series.

Overall, there is potential for error within these picks. The transition zones between the lower coal zone, barren series, and upper coal zones are not sharp, defined contacts, but rather gradational changes in facies. Due to this, there is potential for ambiguity in the picks.
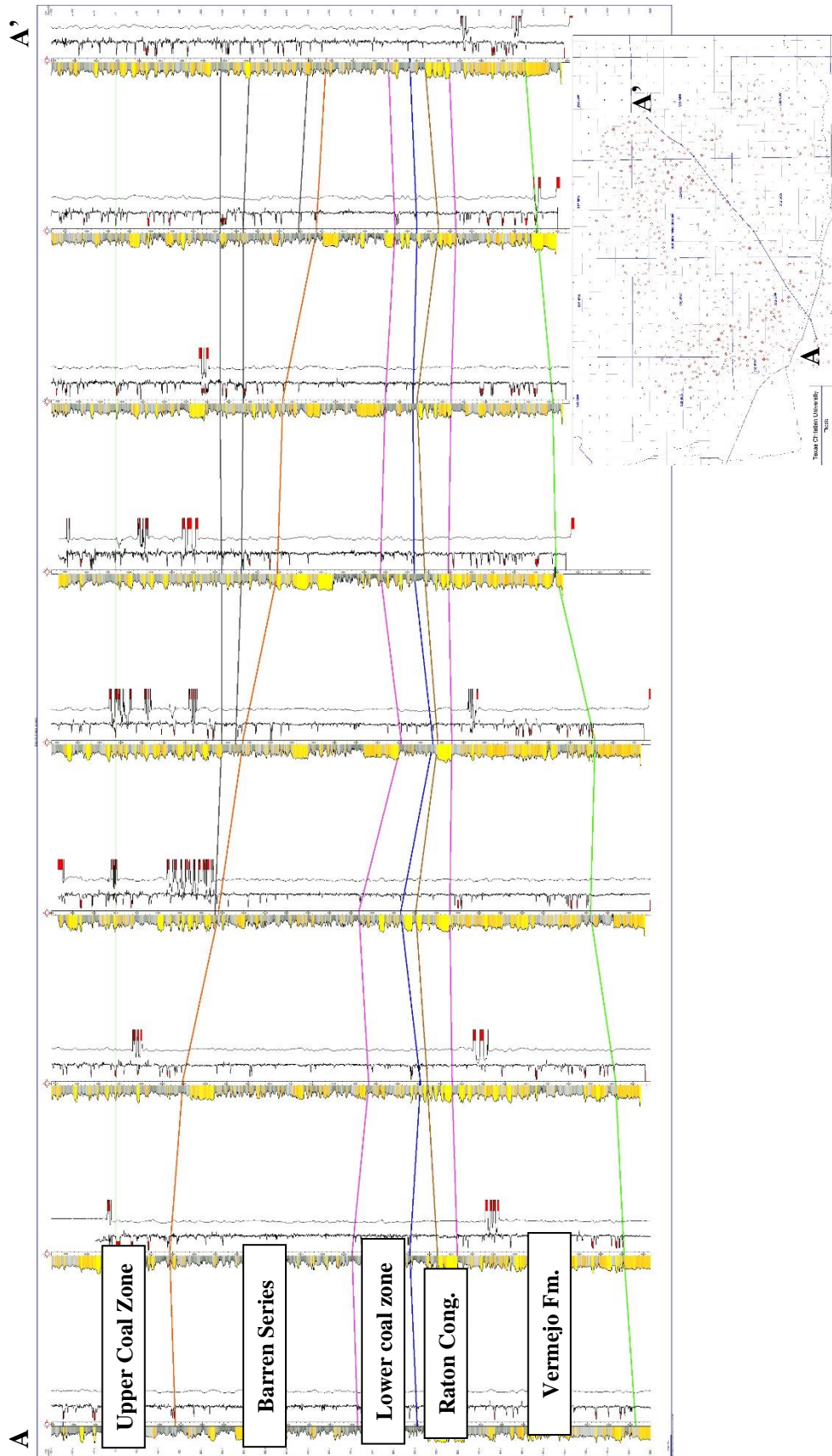
Figure 12: Cross Section from the southwest to the northeast across the study area and locator map. Each well is displaying gamma ray, density, and deep resistivity. The gamma ray log is on track one. API values lower than 100 units are color filled with yellow. Values higher than 100 units are color filled with gray. The density log is on track two. The red color fill indicates values lower than 2 g/cc. The deep induction resistivity log is on the third track. The red color fill indicates values greater than 1000 ohms. The cross section is hung off the coal x datum.

Coal X to Vermejo Maps:

The coal x to Vermejo isopach map (Figure 13) represents the total rock thickness between the coal x coal and the top of the Vermejo Formation. This interval includes the Raton conglomerate, the lower coal zone, the barren series, and the interval of the upper coal zone between the top of the barren series and coal x. The coal x datum was used because the top of the Raton Formation is eroded in the southern and eastern portions of the study area. Coal x is the highest continuous marker bed in the upper coal zone. However, because the coal x is the upper marker, approximately 50 feet to 75 feet of the uppermost Raton Formation from the part of the upper coal zone above coal x is not included in this map. The Blue colors indicates less thickness and yellow indicates more thickness. Contours are on a 25-foot interval. The isopach map shows two distinct thickness trends running roughly northwest-southeast throughout the central portion of the study area. Thicknesses throughout the study area varies between 750 feet and 825 feet. Overall, there is no broad thickness trend. There is a modest thickening in the southwestern corner where the barren series is thick (see below), and a general thickening in the northeastern corner that incorporates most of the units.
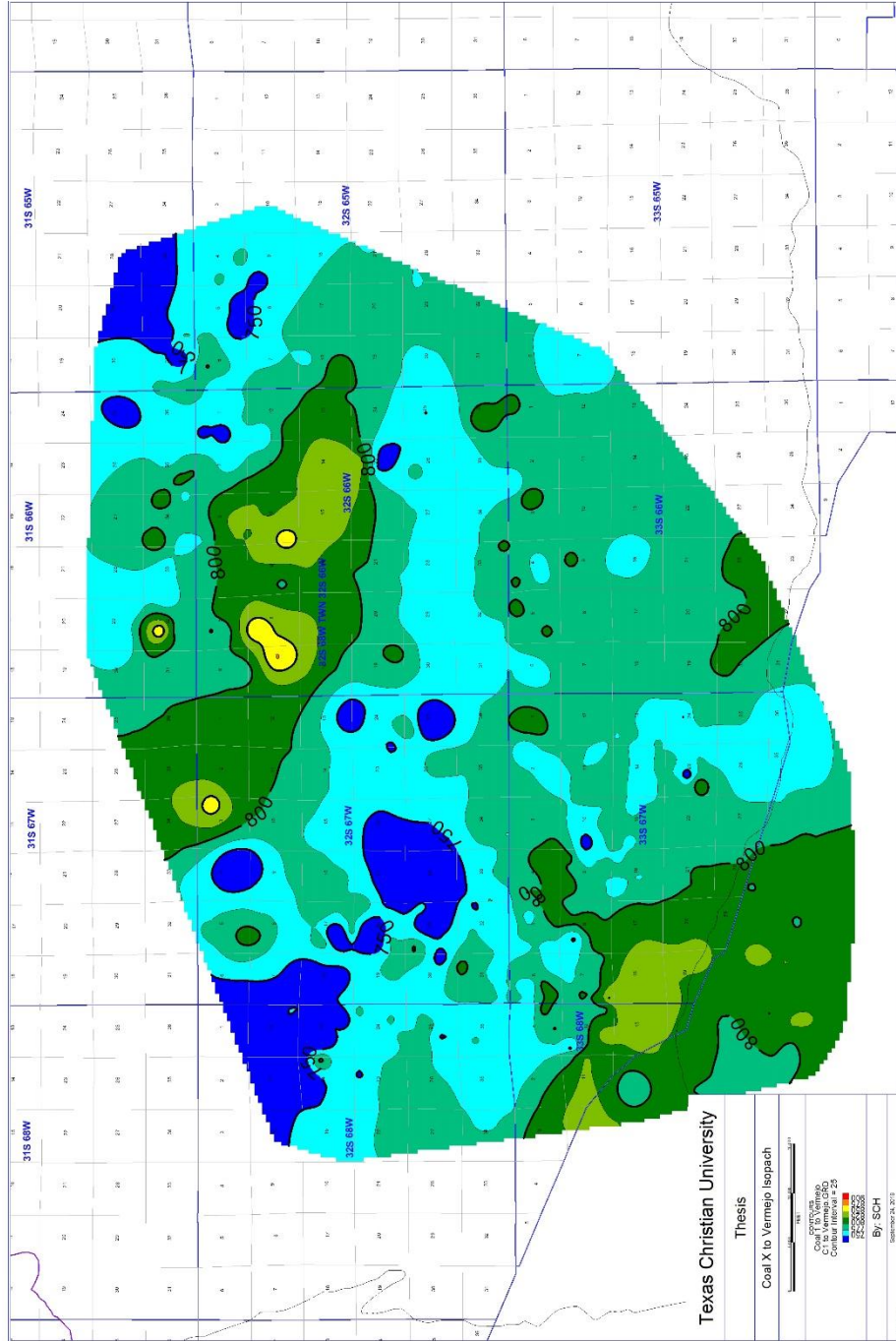
Figure 13: Isopach map of the interval between coal x and the Vermejo Fm. top. The Blue colors indicates less thickness and yellow indicates more thickness. Contours are on a 25-foot interval.

Raton Conglomerate Maps:

The Raton conglomerate isopach map (Figure 14) represents the total rock thickness between the Raton conglomerate top and the Vermejo top. The blue color indicates where the interval is thinner. The yellow indicates greater thickness. Contours are on a 10-foot interval. Thicknesses range from 10 feet to 130 feet. The conglomerate is thickest in the western portion of the study area and thins in a radial fashion throughout the rest of the study area. The thinning is gradual to the northeast and the southwest, but becomes more dramatic towards the southeastern portion of the study area.

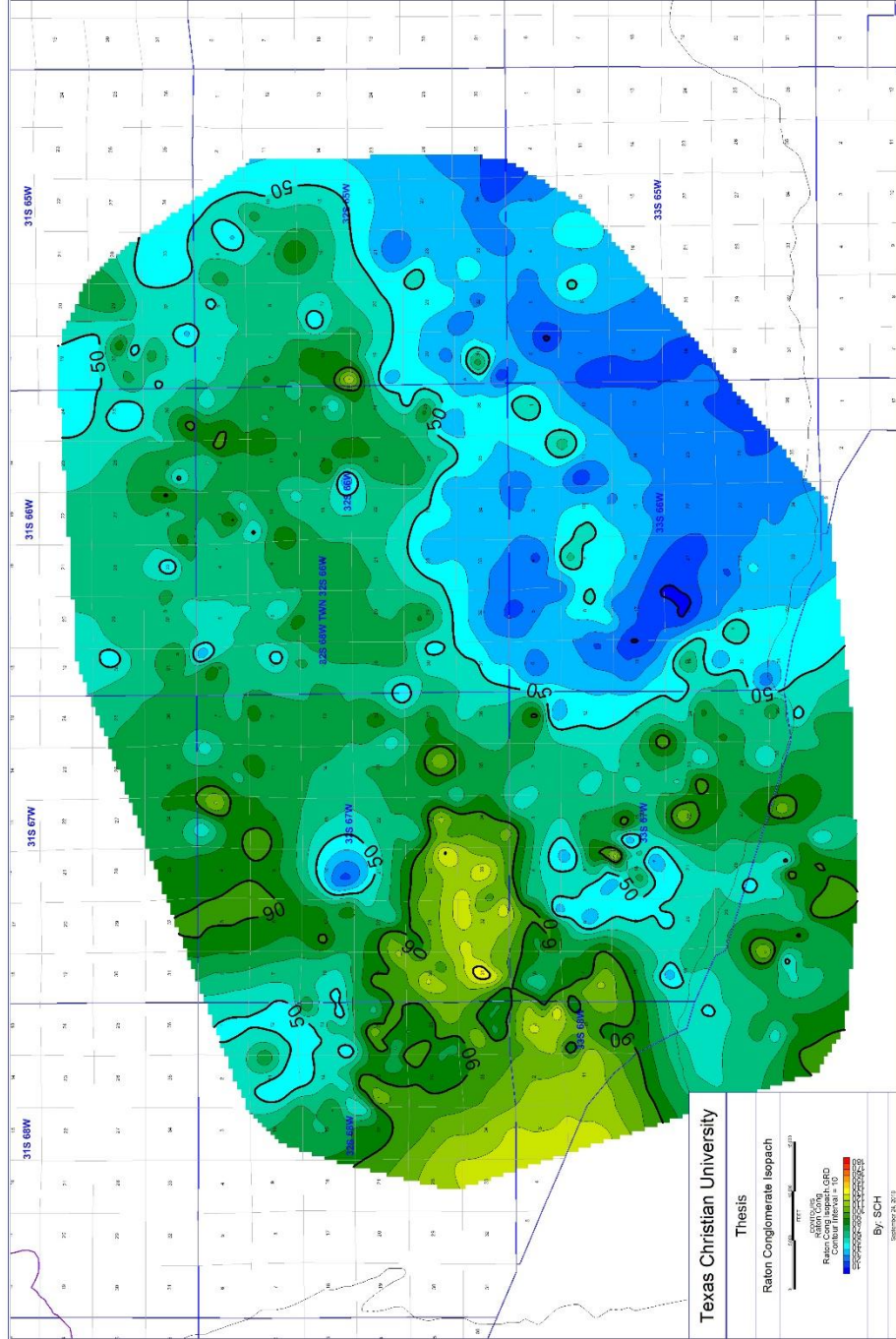**Figure 14: Isopach map of the Raton Conglomerate. The blue color indicates where the interval is thinner. The yellow indicates greater thickness. Contours are on a 10-foot interval.**

Lower coal zone Maps:

The lower coal zone isopach map (Figure 15) represents the total rock thickness between the lower coal zone top and the lower coal zone base. Contours are on a 25-foot interval and the unit ranges from 75 feet to 200 feet at its thickest. The blue indicates areas where the lower coal zone interval is thinner while the yellow and orange indicates greater thickness. Overall, there is a thinning trend to the east and southeast. However, throughout the study area there appears to be a lattice of thicks and thins. To the southeast, the map shows a large area where the lower coal zone is thin. This is likely because Petra is trying to extrapolate data into an area where the lower coal zone is not penetrated and cannot be correlated.

The lower coal zone coal percentage map (Figure 16) measures the percentage of the total rock thickness within the lower coal zone that is made up of the coal lithofacies. Contours are on a 1% interval and range from 0% to 15%. The green indicates areas where there is a lower percentage of coal while the orange and red indicates a higher percentage of coal. The coal distribution within the lower coal zone appears to be sporadic throughout the study area. In the southern portion of the study area there is a north-south trend with low coal abundances. In the northwestern portion of the study area, coal percentages vary widely and abruptly. Throughout the study area, predominantly in the northwest and northeast, there are large red "bullseyes" indicating high coal abundances. However, within these red "bullseyes" there are no wells. This indicates that Petra's contouring algorithm has extrapolated data creating a false high abundance.

The lower coal zone sandstone percentage map (Figure 17) measures the percentage of the total rock thickness that is composed of the sandstone lithofacies within the lower coal zone. Sand percentages range from 15% to 35%. The green indicates areas where there is a lower percentage

of sand while the orange and red indicates a higher percentage of sand. The sandstone percentage map displays two distinct high percentage trends. The northern trend begins in the western portion of the study area and continues to the north. The southern trend begins in the southwestern portion of the study area and continues to the northeast, ultimately dying out in the northeastern quadrant of the map. The higher sandstone percentages are roughly inverse to the higher coal percentages identified in the lower coal zone coal percentage map.

The lower coal zone 1 ft to 5 ft sandstone frequency map (Figure 18) displays the number of sand intervals that are between 1 ft and 5 ft thick within the lower coal zone interval. Sandstone frequencies range from 0 to 7 individual sandstone beds. The green indicates areas where there is a lower amount of sand intervals while the orange and red indicates a higher amount of sand beds. This map does not imply whether or not the sands can be correlated, but is just a count. These thin sandstones are most frequent in the southern portion of the map, form a channel-like geometry along a north-south trend, and lie within the same area as the trends present on figure 17. There are higher concentrations of 1 foot to 5 feet sandstones scattered throughout the northern portion of the study area indicated by the red dots. The large abundance (circled on map) in the northern portion of the map is a contouring error from Petra's contouring algorithm and should be ignored throughout the remaining maps. This error is created by the Petra's contouring algorithm trying to extrapolate data across areas where there is little to no well control.

The lower coal zone 5 ft to 10 ft sandstone frequency map (Figure 19) measures the number of sandstone intervals that are between 5 ft and 10 ft thick within the lower coal zone interval. Sandstone frequencies range from 0 to 3 individual sandstone beds. The green indicates areas where there is a lower number of sand intervals while the red indicates a higher number of sand beds. These thicker sandstones occur predominantly along the edges of the study area with one 5 to 10 ft sandstone found in the center. The abundance in the northern and eastern portion of the map is a contouring error from Petra's contouring algorithm and should be ignored throughout the remaining maps.
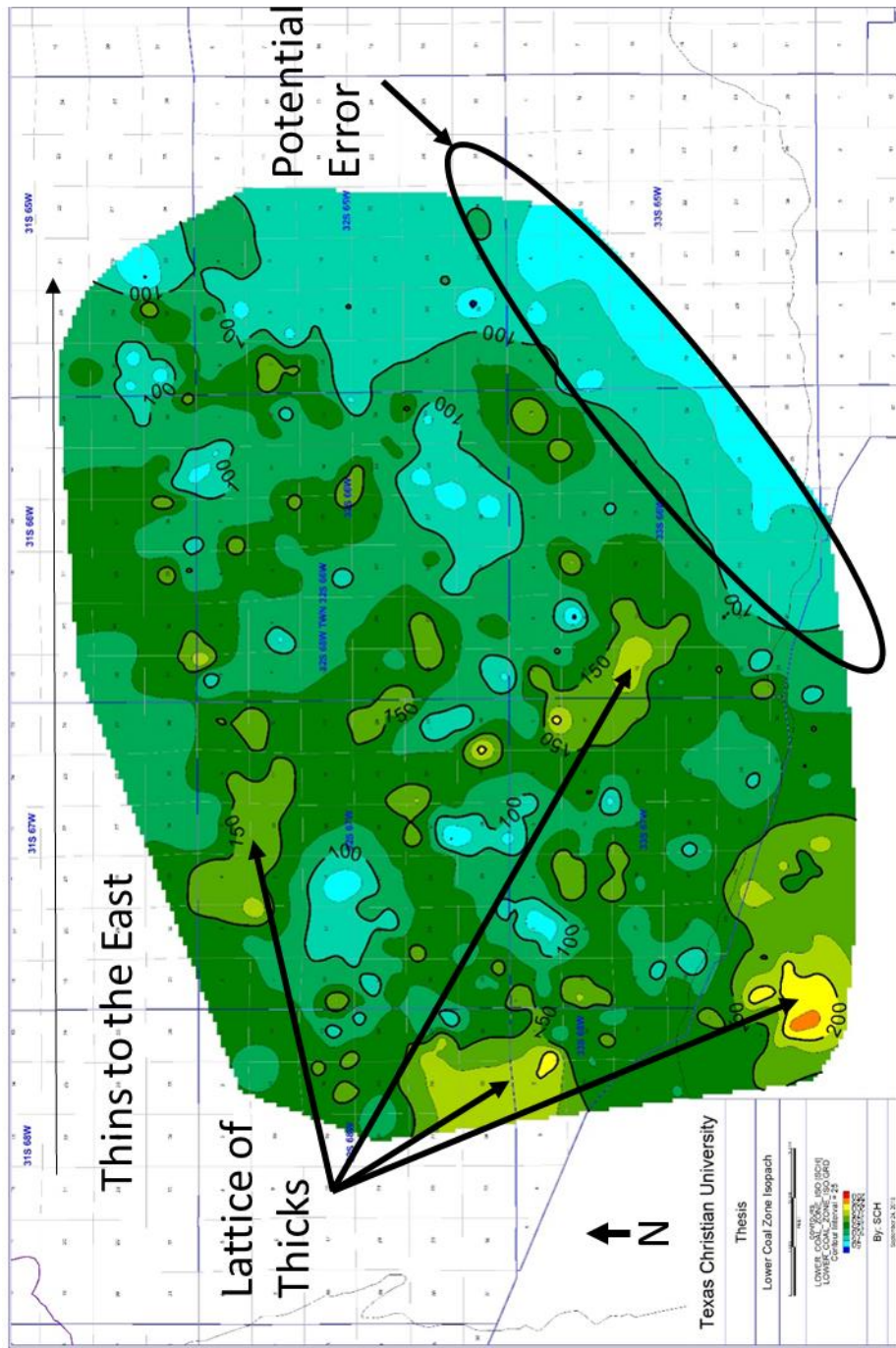
Figure 15: Isopach map of the lower coal zone. Contours are on a 25-foot interval and the unit ranges from 75 feet to 200 feet at its thickest. The blue indicates areas where the lower coal zone interval is thinner while the yellow and orange indicates greater thickness.
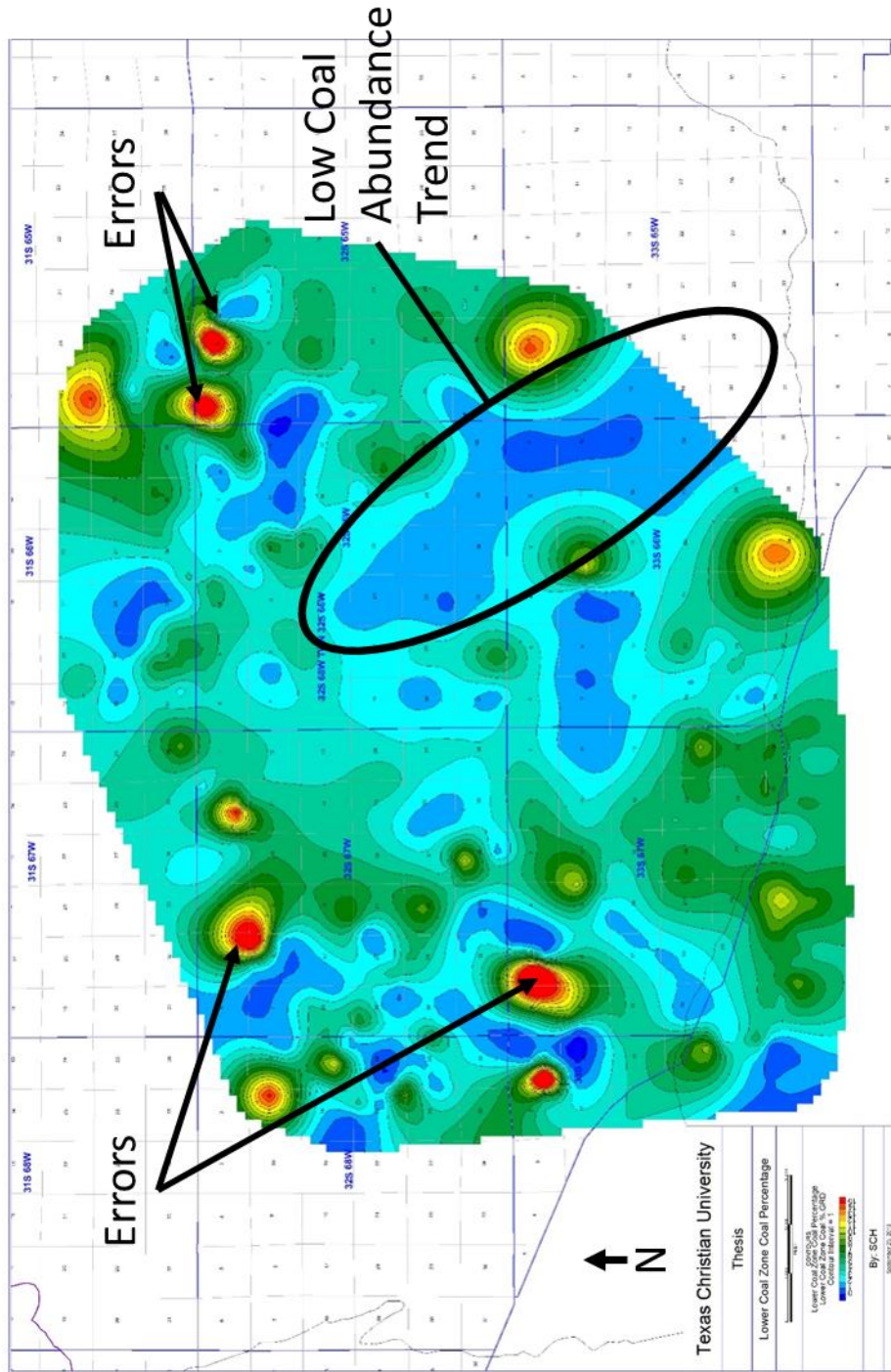
Figure 16: A percent coal map of the lower coal zone. Contours are on a 1% interval and range from 0% to 15%. The green indicates areas where there is a lower percentage of coal while the orange and red indicates a higher percentage of coal.

Figure 17: A percent sand map of the lower coal zone. Contours are on a 5% interval and range from 15% to 35%. The green indicates areas where there is a lower percentage of sand while the orange and red indicates a higher percentage of sand.
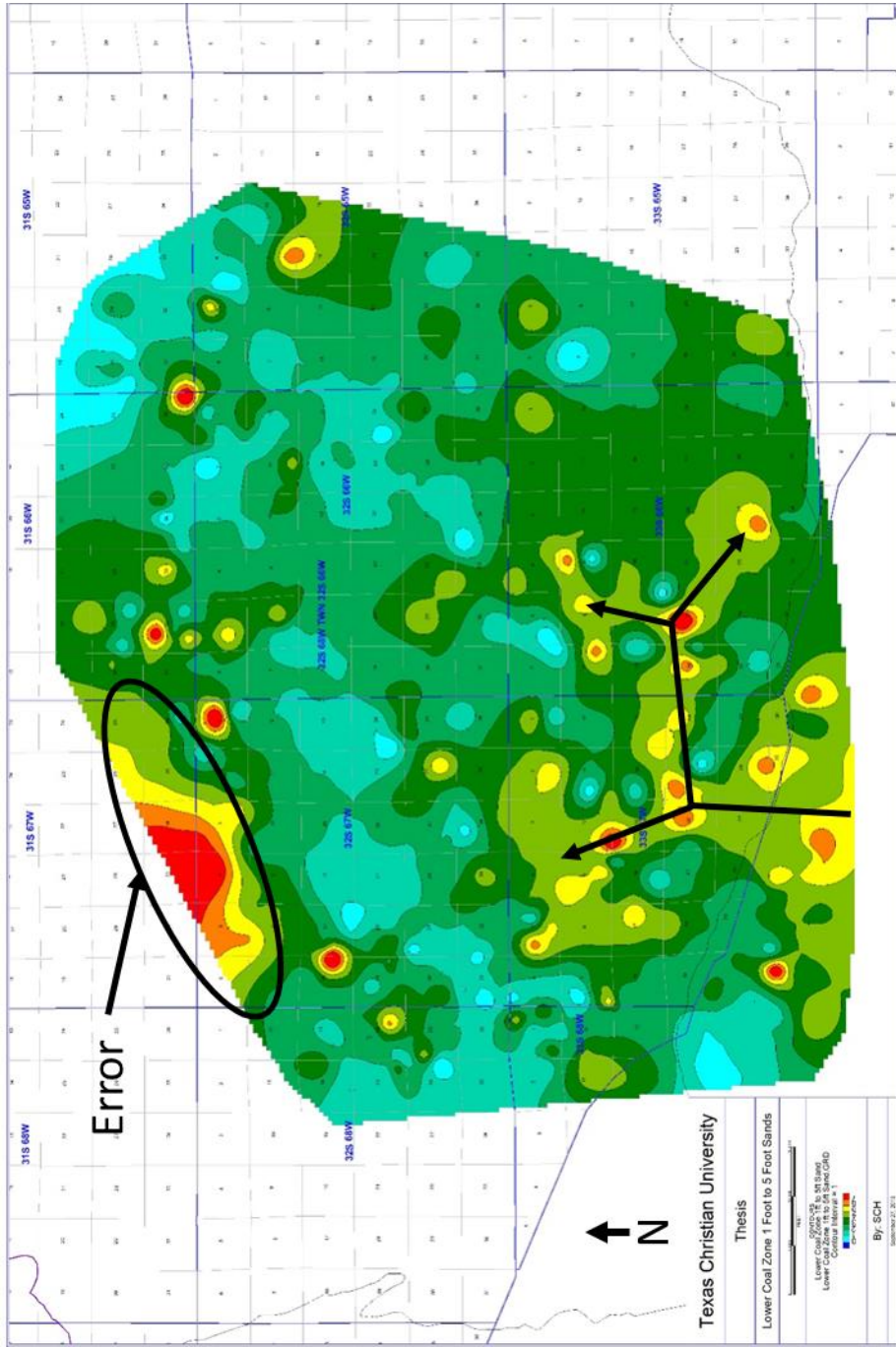
Figure 18: Frequency map of the number of sand intervals between 1ft and 5ft thick within the lower coal zone. Contours are on a one frequency interval and range from 0 to 7 individual sandstone beds. The green indicates areas where there is a lower amount of sand intervals while the orange and red indicates a higher amount of sand beds.
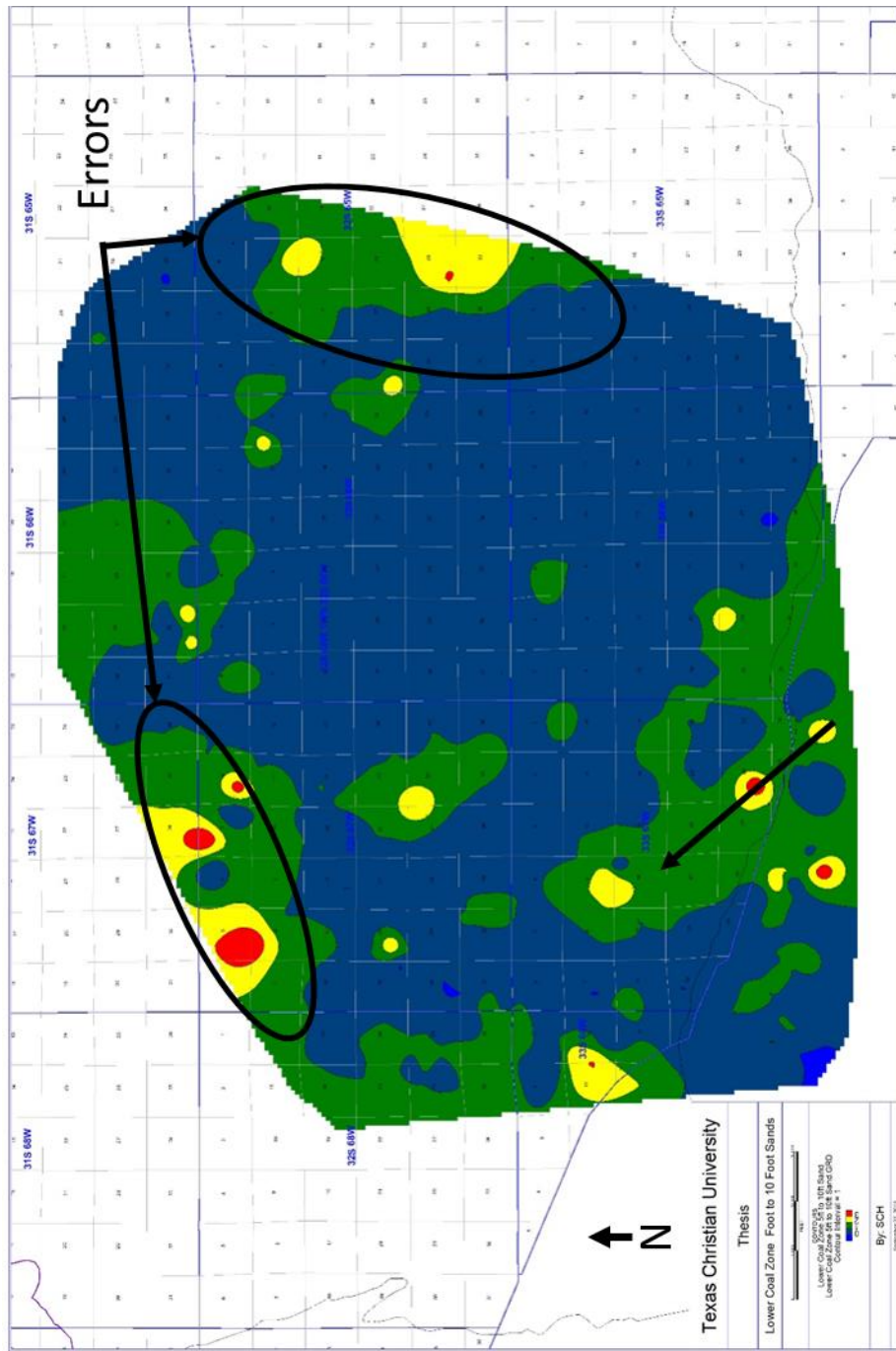
Figure 19: Frequency map of the number of sand intervals between 5ft and 10ft thick within the lower coal zone. Contours are on a 1 frequency interval and range from 0 to 3 individual sandstone beds. The green indicates areas where there is a higher number of sand intervals while the red indicates a lower number of sand beds

Barren Series Maps:

The barren series isopach map (Figure 20) measures total rock thickness between the barren series top to the top of the lower coal zone. Thicknesses range from 200 feet to 650 feet. The blue indicates areas where the barren series is thinner while the green indicates greater thickness. An area of greater thicknesses present in the southwestern portion of the map that spans to the northeast and has a generally conical mounded form. There is another area of greater thickness in the southern portion of the map that extends to the north and ultimately combines with the southwestern thickness trend. The barren series interval thins to the northwest and to the east. Thinning to the northeast is much more dramatic than the thinning to the southeast.

The barren series coal percentage map (Figure 21) displays the percentage of the total rock thickness that is composed of the coal lithofacies. Percentages range from 0% to 6%. The green indicates areas where there is a lower percentage of coal whi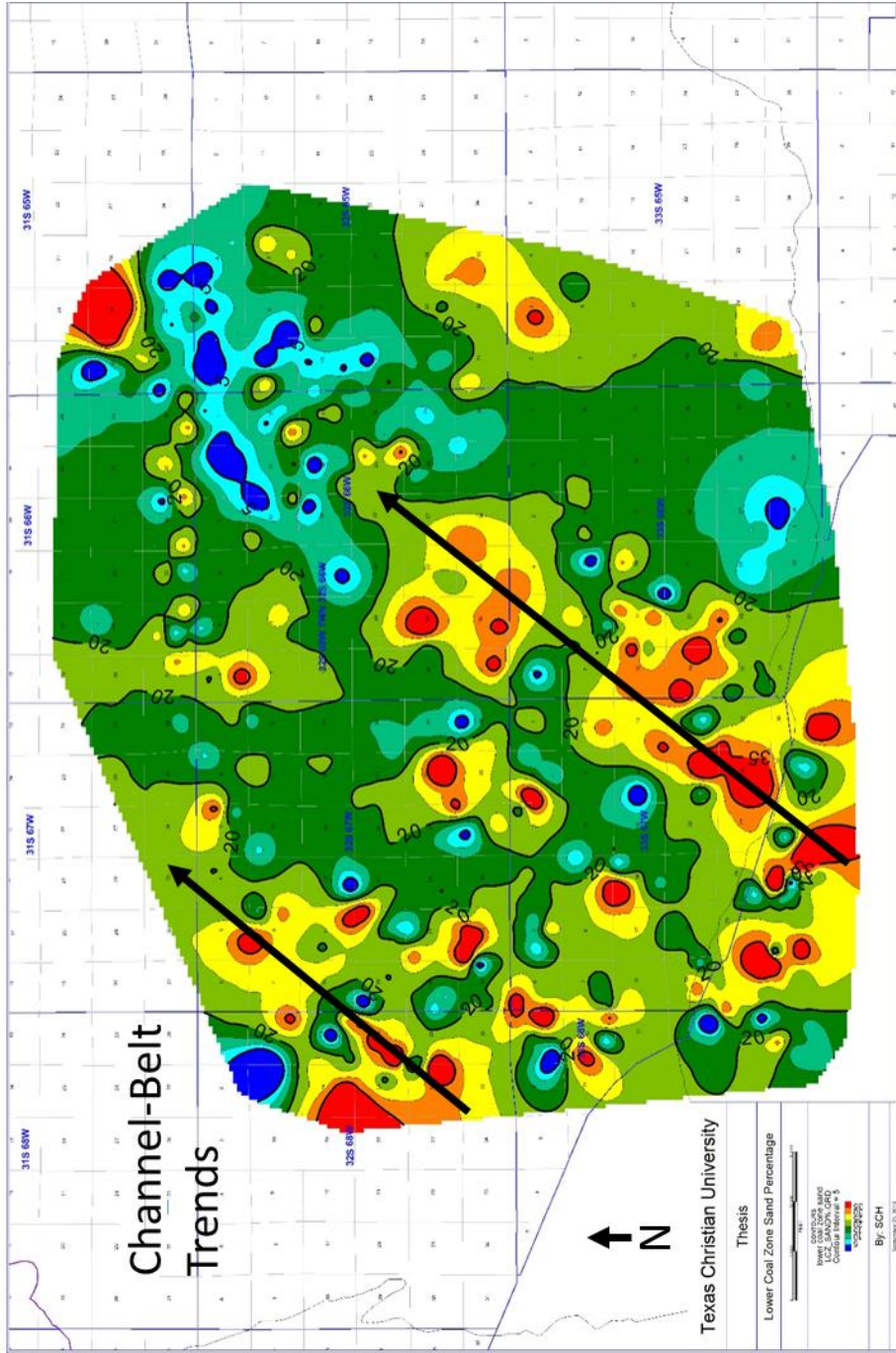le the orange and red indicates a higher percentage of coal. Throughout the center of the basin, the barren series contains at least 1% of coal. The majority of the coal lies within the northern and northeastern portion of the study area.

The barren series sandstone percentage map (Figure 22) displays the percentage of the total rock thickness that is composed of the sandstone lithofacies. Percentages range from 15% to 55%. The green indicates areas where there is a lower percentage of sand while the orange and red indicates a higher percentage of sandstones. Sandstones are widespread throughout the interval of interest with higher sandstone concentrations in the southern portion of the study area. Due to the difference in thickness throughout the barren series, there might be artifact within this map. This is because lower quantities of sand have a higher influence over the sand percentages in areas where the barren series interval is less thick. The reason for this is that the sand percentage maps are derived by dividing total interval sand thickness by total interval thickness. There is a slight

tendency for higher concentrations of sandstone to occur within the thicker parts of the barren series to the south and southwest. This trend is not exclusive, however, as higher percentages of sandstone are present in the northeastern portion of the study area where the barren series is generally thin.

The following interval maps, excluding the 10ft to 15ft sandstone frequency map, are all contoured on a 1 sand interval. The 10 ft to 15 ft sand map is contoured on a 2 sand interval. The sand intervals are determined by using a less than 100 API unit cutoff on the gamma ray log. Sands are counted when an interval with a gamma reading below 100 API units falls within the thickness constraints. For example, for a sandstone to be counted on the 5 ft to 10 ft interval map, there must be an interval reading below 100 API units that is between 5 to 10 feet thick. Green color fill on the map indicates areas where there is a lower count of sand intervals. Reds and oranges indicate areas where there is a higher concentration of sand intervals. These maps do not imply whether or not the sands can be correlated, but is just a count

The barren series 1 ft to 5 ft sandstone frequency map (Figure 23) displays the number of sandstone intervals that are between 1 ft and 5 ft thick within the barren series interval. The most frequent sandstones lie within the southern and central portions of the study area, with substantially fewer thin sandstones in the northeastern portion of the study area. There are two major high frequency trends. The first is in the southwestern corner of the area and extends to the north. The second is found in the southeastern portion of the area and extends towards the north-northeast. These two trends generally follow the trends of greatest thickness in the barren series (Figure 20). The lower frequency of thin sandstones in the eastern portion of the map also reflects the lower barren series thicknesses in this portion of study area. The total percent sandstone (Figure 22) is low here but not substantially lower than in the southwest.

The barren series 10 ft to 15 ft sandstone frequency map (Figure 24) shows the number of sandstone intervals that are between 10 ft and 15 ft thick within the barren series interval. Sandstones of this thickness are predominantly located in the western portion of the study area. There are two diverging trends extending from the southwest and one shorter body extending from the northeast. These sandstones create a channel like geometry throughout the study area. The large area of red and yellow in the eastern portion of the map appears to be an extrapolation error. This is because there are few wells in this area of the map and there is not a well present within the red color fill.

The barren series 15 ft to 20 ft sandstone frequency map (Figure 25) displays the number of sandstone intervals that are between 15 ft and 20 ft thick within the barren series interval. Sandstones of this scale are predominantly within the southern and western portion of the map on a north-south trend. This trend is consistent with the trends in figure 24.
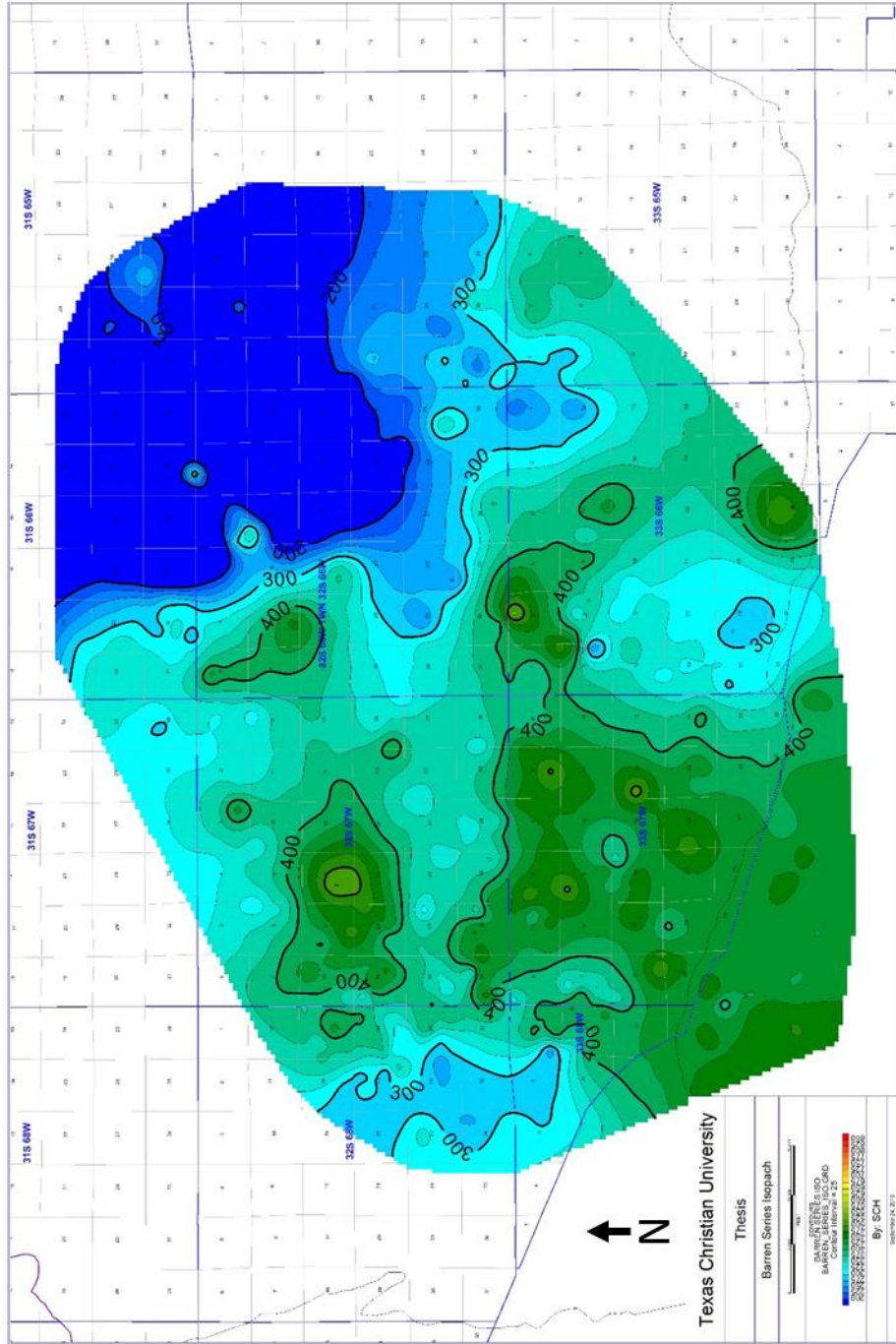
Figure 20: An isopach map of the barren series interval. . Contours are on a 25 ft interval and range from 200 feet to 650 feet. The blue indicates areas where the barren series is thinner while the green indicates greater thickness
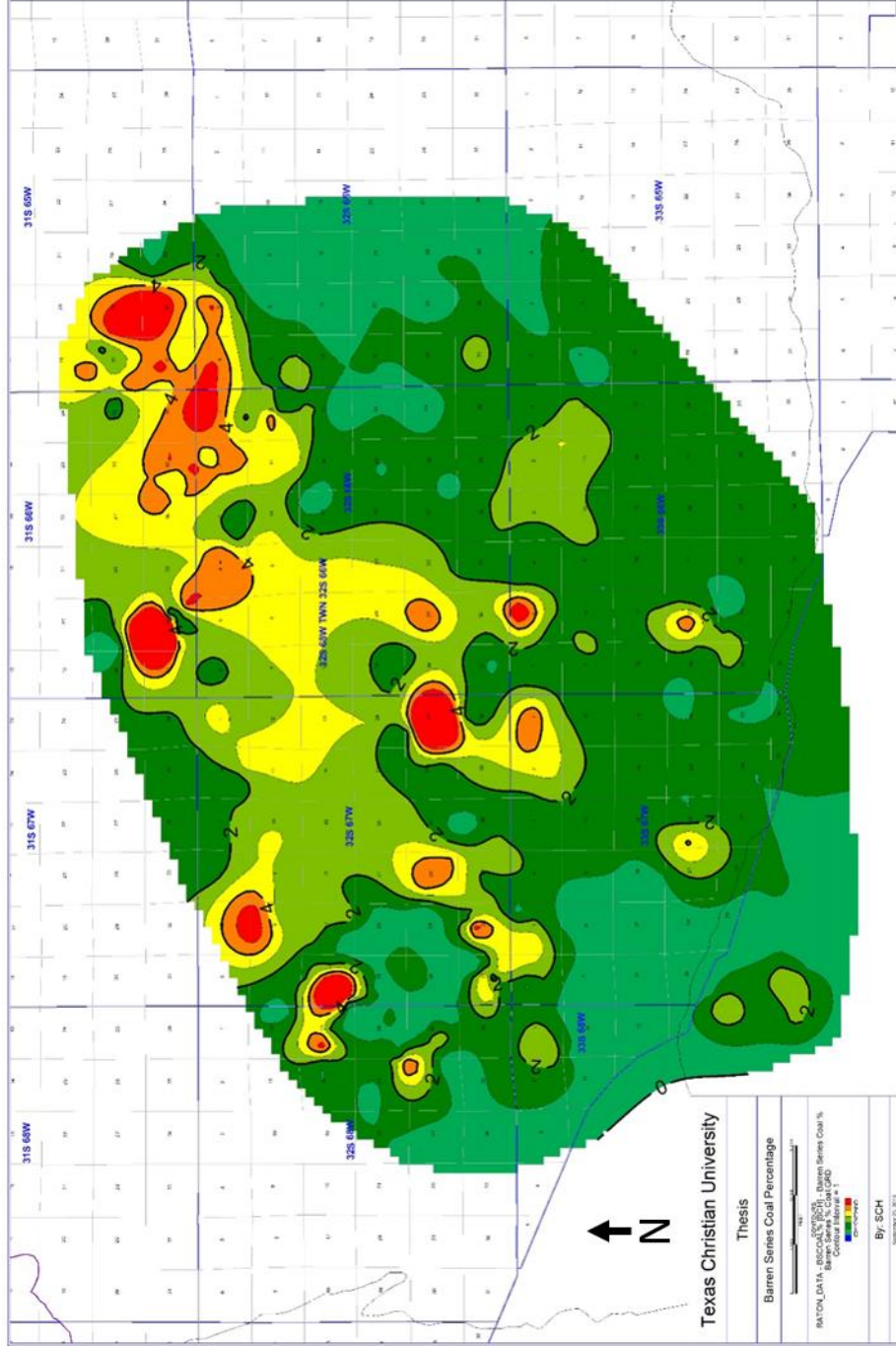
Figure 21: A percent coal map of the barren series. Contours are on a 1% interval ranging from 0% to 6%. The green indicates areas where there is a lower percentage of coal while the orange and red indicates a higher percentage of coal.
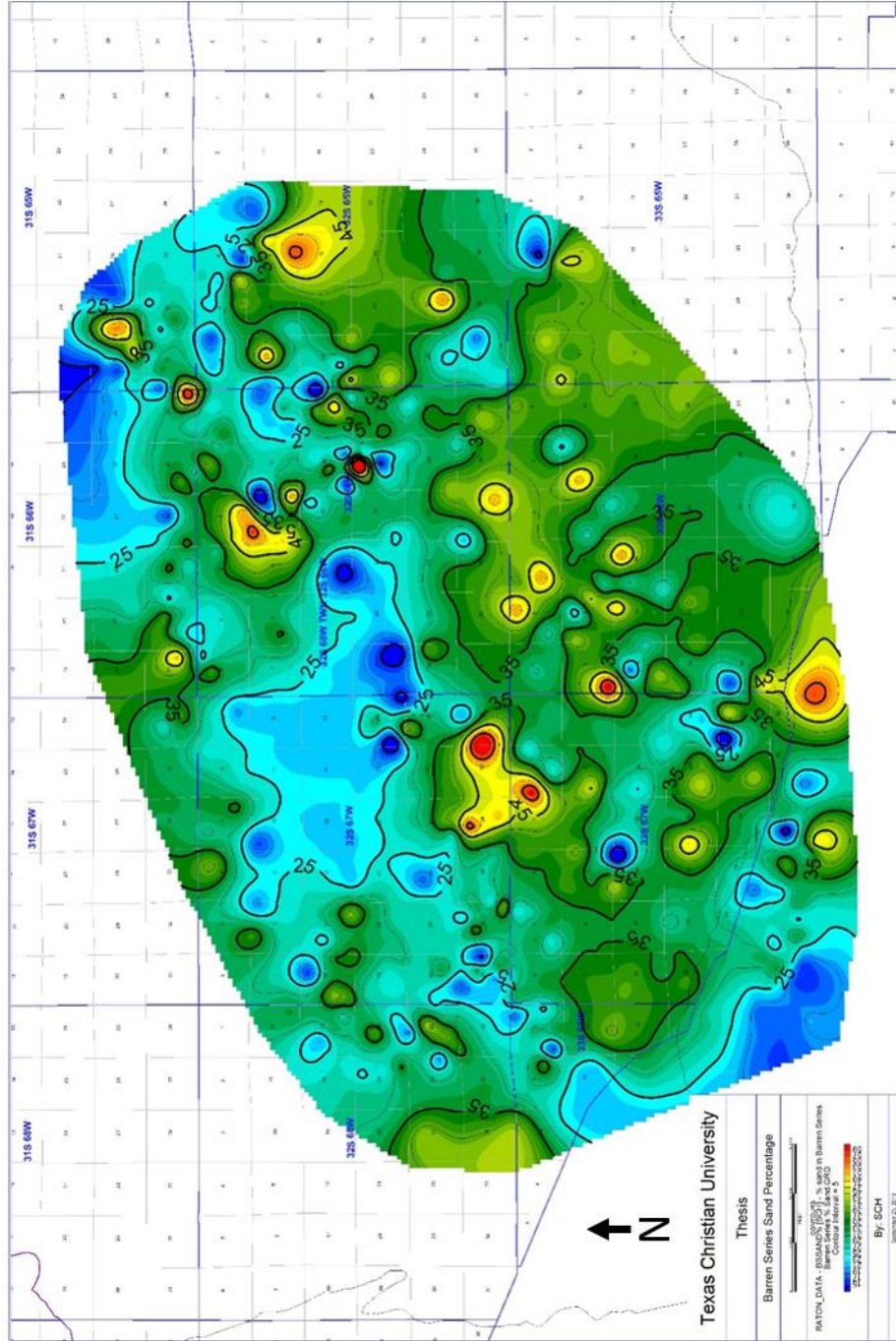
Figure 22: A percent sand map of the barren series. Contours are on a 5% interval and range from 15% to 55%. The green indicates areas where there is a lower percentage of sand while the orange and red indicates a higher percentage of sand stones.

Figure 23: Frequency map of the number of sand intervals between 1ft and 5ft thick within the barren series. Contours are on a 1 frequency interval and range from 4 to 32 sandstones. Green color fill on the map indicates areas where there is a lower count of sand intervals. Reds and oranges indicate areas where there is a higher concentration of sand intervals.

Figure 24: Frequency map of the number of sand intervals between 10ft and 15ft thick within the barren series. Contours are on a 2 frequency interval and range from 0 to 28 sandstones. Green color fill on the map indicates areas where there is a lower count of sand intervals. Reds and oranges indicate areas where there is a higher concentration of sand intervals.

Figure 25: Frequency map of the number of sand intervals between 15ft and 20ft thick within the barren series. Contours are on a 1 frequency interval and range from 0 to 3 sandstones. Green color fill on the map indicates areas where there is a lower count of sand intervals. Reds and oranges indicate areas where there is a higher concentration of sand intervals.

Coal X to Barren Series Maps:

The coal x to barren series isopach map (Figure 26) displays the total rock thickness between the coal x top and the top of the barren series. Thicknesses range from 100 feet to 500 feet. The blue indicates areas where the interval is thinner while the yellow and orange indicates areas where the thickness is greater. The contours display an overall thickening to the northeastern and eastern portions of the area. In the southwestern portion of the study area, there is a north-south trend of lower thicknesses. In the northwest, there is an area of greater thickness.

The coal x to barren series sandstone percentage map (Figure 27) shows the percentage of the total rock thickness composed of sandstone lithofacies. Percentages range from 10% to 50%. The green indicates areas where there is a lower percentage of sand while the orange and red indicates a higher percentage of san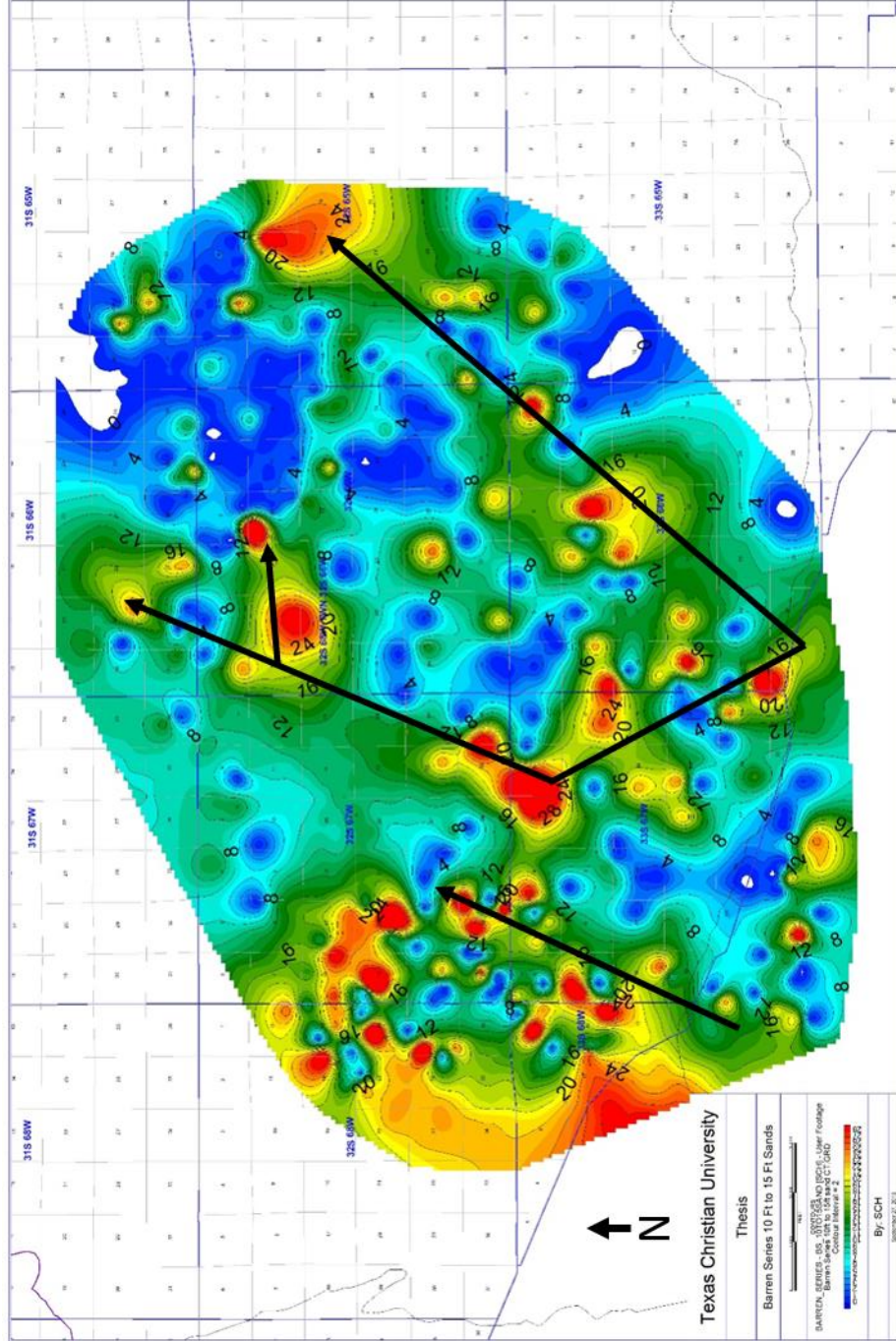d. In the northern portion of the map there is an artifact created by Petra's contouring algorithm. It is likely due to a lack of well control and Petra trying to extrapolate data across an area without data. Sandstones are widespread throughout the interval. A fairway of high sandstone content extends from the southern to northeastern portion of the study area. There also appears to be a smaller north-south trend in the western portion of the area. Due to the difference in thickness interval throughout the interval of interest, there might be error within this map. This is because similar quantities of sand have a higher influence over areas of less thickness displaying a higher sand content on the map because the sand content percentage is derived by dividing overall sand thickness by total interval thickness. This may account for the general lack of sandstone over the top of the barren thick area. The trends however are discrete within the low thickness regions and are not an artifact. The eastern trend follows the southeastern edge of the thick-mounded section in the barren series isopach map (Figure 20). The western trend is just off this mound to the north.

The coal x to barren series coal percentage map (Figure 28) displays the percentage of the total rock thickness that is composed of the coal lithofacies. Percentages range from 0% to 10%. The blue indicates areas where there is a lower percentage of coal while the orange and red indicates a higher percentage of coal. Throughout the center of the basin, the interval between the coal x and barren series contains at least 1% coal. The majority of the coal is found along the northern edge of the area. However, there is also a slightly higher percentage of coal found in the eastern portion of the study area. Inversely, there is a southeast-northwest trend of low coal abundances. The areas of higher coal concentrations are inverse of those areas of higher sandstone concentrations. The red highs are potentially areas of error as there is not a well these red highs.

The following interval maps define the number of sands beds of a respective thickness and are all contoured on a 1 sand interval. The sand intervals are determined by using a less than 100 API unit cutoff on the gamma ray log. Sands are counted when an interval with a gamma reading below 100 API units falls within the thickness constraints. For example, for a sand to be counted on the 5 ft to 10 ft interval map, there must be an interval reading below 100 API units that is between 5 to 10 feet thick. Green color fill on the map indicates areas where there is a lower count of sand intervals. Reds and oranges indicate areas where there is a higher concentration of sand intervals. These maps do not imply whether or not the sands can be correlated, but is rather just a count

The coal x to barren series 1 ft to 5 ft sandstone frequency map (Figure 29) shows the number of sandstone intervals that are between 1 ft and 5 ft thick within the coal x to barren series interval. These thinner sandstones are most frequent within the eastern portion of the study area, with substantially fewer thin sandstones in the western portion of the area. However, the lower number of sandstones may be because the interval of interest is thinner in the western portion of

the basin. Sandstone patterns are generally dispersed in this area and do not appear to follow discrete linear trends. The highest occurrence of these thin sandstones is generally outside and east of the axis of highest total sandstone percent (Figure 27).

The coal x to barren series 5 ft to 10 ft sandstone frequency map (Figure 30) displays the number of sandstone intervals that are between 5 ft and 10 ft thick within the coal x to barren series interval. Sandstones between 5 to 10 ft thick are predominantly located in the western portion of the study area. There is one major north-south trend starting in the southwest and extending to the northwestern portion of the study area. A second trend starts in the south and extends to the northeast before dying out in the eastern portion of the map. In the eastern portion of the study area, there are substantially fewer sandstones between 5 and 10 ft thick.

The coal x to barren series 10 ft to 15 ft sandstone frequency map (Figure 31) displays the number of sandstone intervals that are between 10 ft and 15 ft thick within the coal x to barren series interval. The majority of the sandstones between 10 and 15 ft thick lie within the eastern portion of the area. However, in the northwestern quadrant of the map there are multiple wells with one or two 10 to 15 ft sandstones. There is thus some dispersion of these locally thick sandstones. The eastern trend of these thick sandstones approximates the trend of the higher percentages of total sandstone in the same area. These thick sandstones generally account for the thick eastern trend with some addition from thinner sandstones.
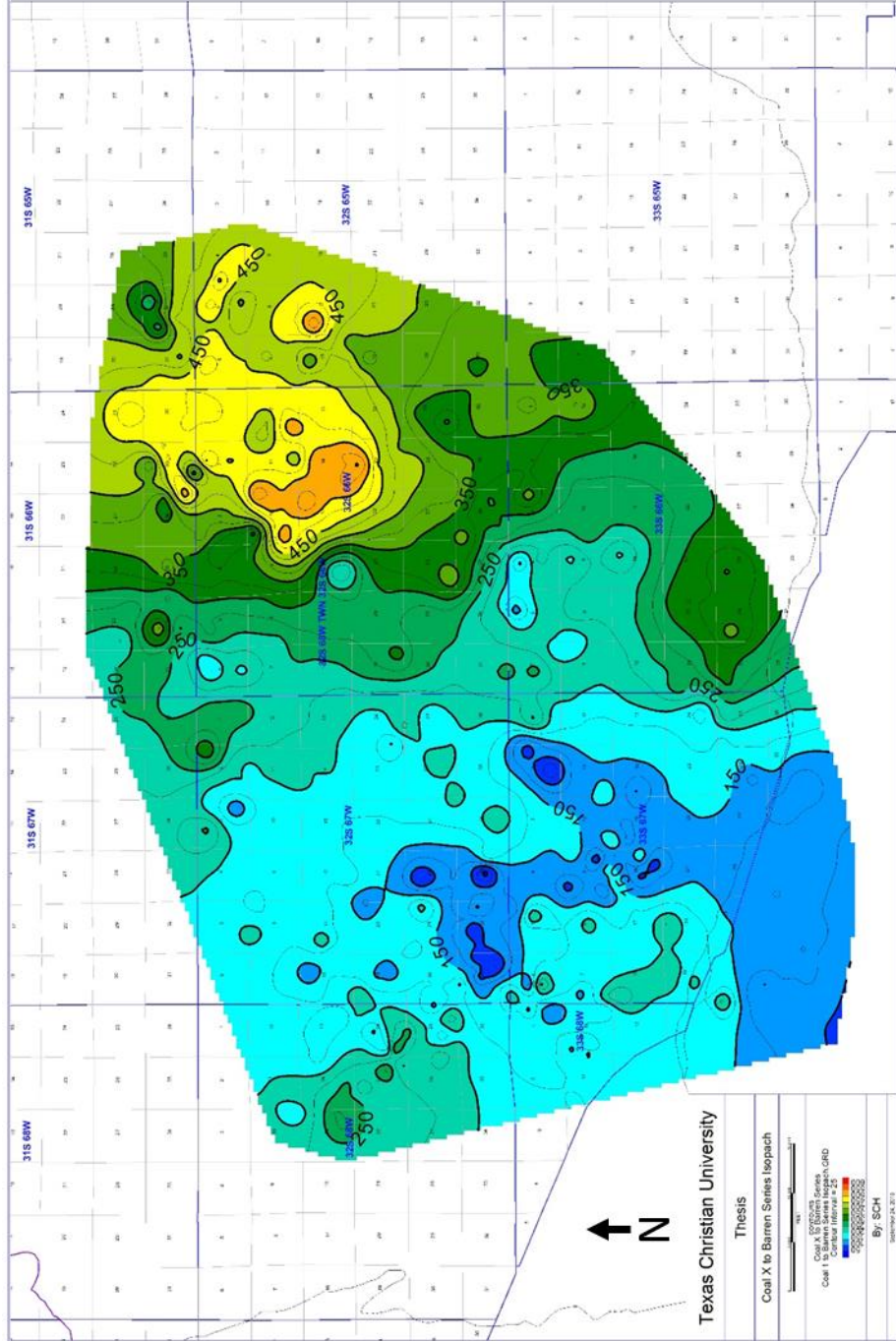
Figure 26: An isopach map of the interval between coal x and the top of the barren series. . Contours are on a 25-foot interval and range from 100 feet to 500 feet. The blue indicates areas where the interval is thinner while the yellow and orange indicates areas where the thickness is greater.

58

Figure 27: A percent sand map of the interval between coal x and the barren series. Contours are on a 5% interval and range from 10% to 50%. The green indicates areas where there is a lower percentage of sand while the orange and red indicates a higher percentage of sandstone.

Figure 28: A percent coal map of the interval between coal x and the barren series. Contours are on a 1% interval and range from 0% to 10%. The green indicates areas where there is a lower percentage of sand while the orange and red indicates a higher percentage of coal.

Figure 29: Frequency map of the number of sand intervals between 1ft and 5ft thick between coal x and the top of the barren series. Contours are on a 1 frequency interval and range from 4 to 32 sandstones. Green color fill on the map indicates areas where there is a lower count of sand intervals. Reds and oranges indicate areas where there is a higher concentration of sand intervals.

Figure 30: Frequency map of the number of sand intervals between 5ft and 10ft thick between coal x and the top of the barren series. Contours are on a 1 frequency interval and range from 1 to 7 sandstones. Green color fill on the map indicates areas where there is a lower count of sand intervals. Reds and oranges indicate areas where there is a higher concentration of sand intervals.
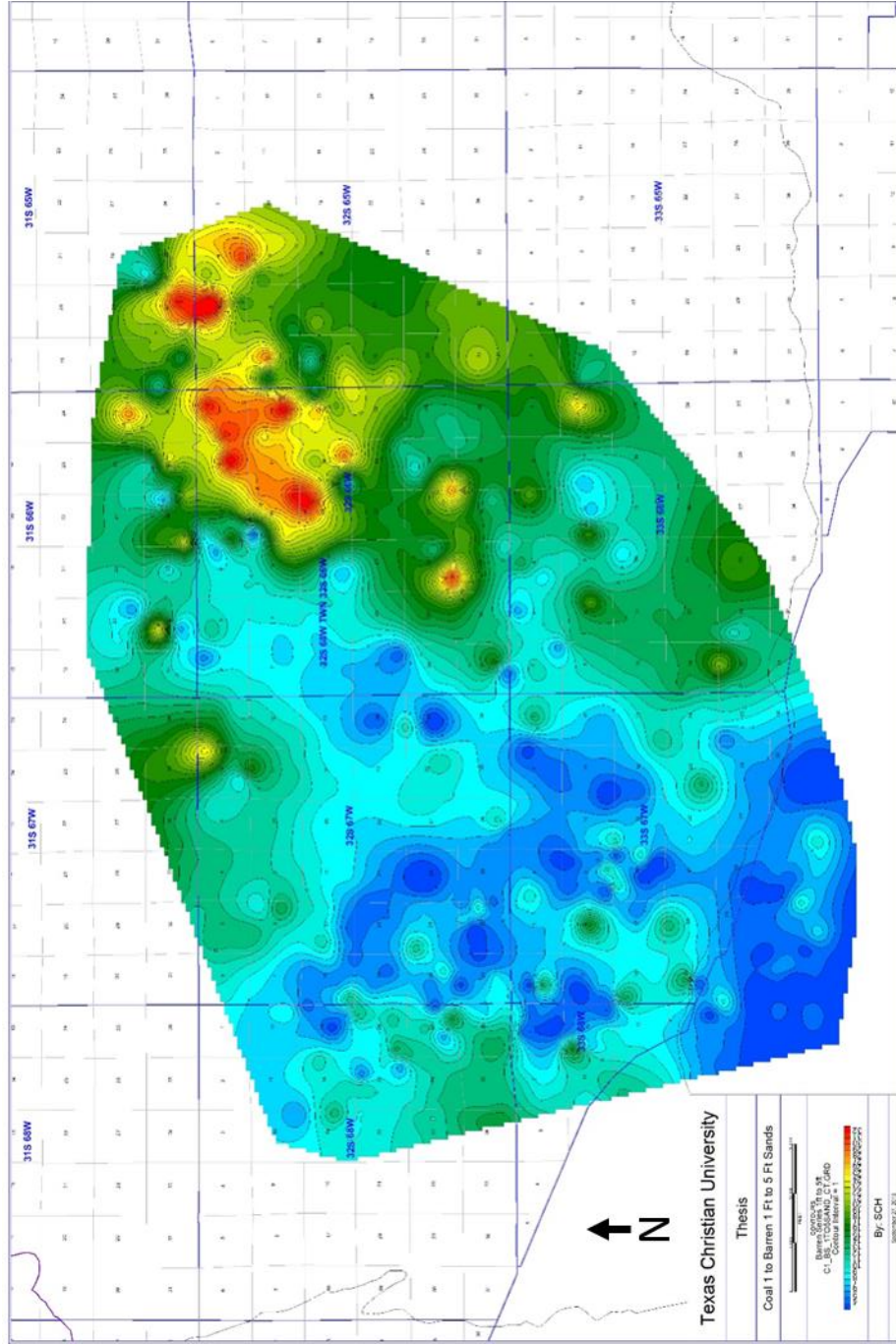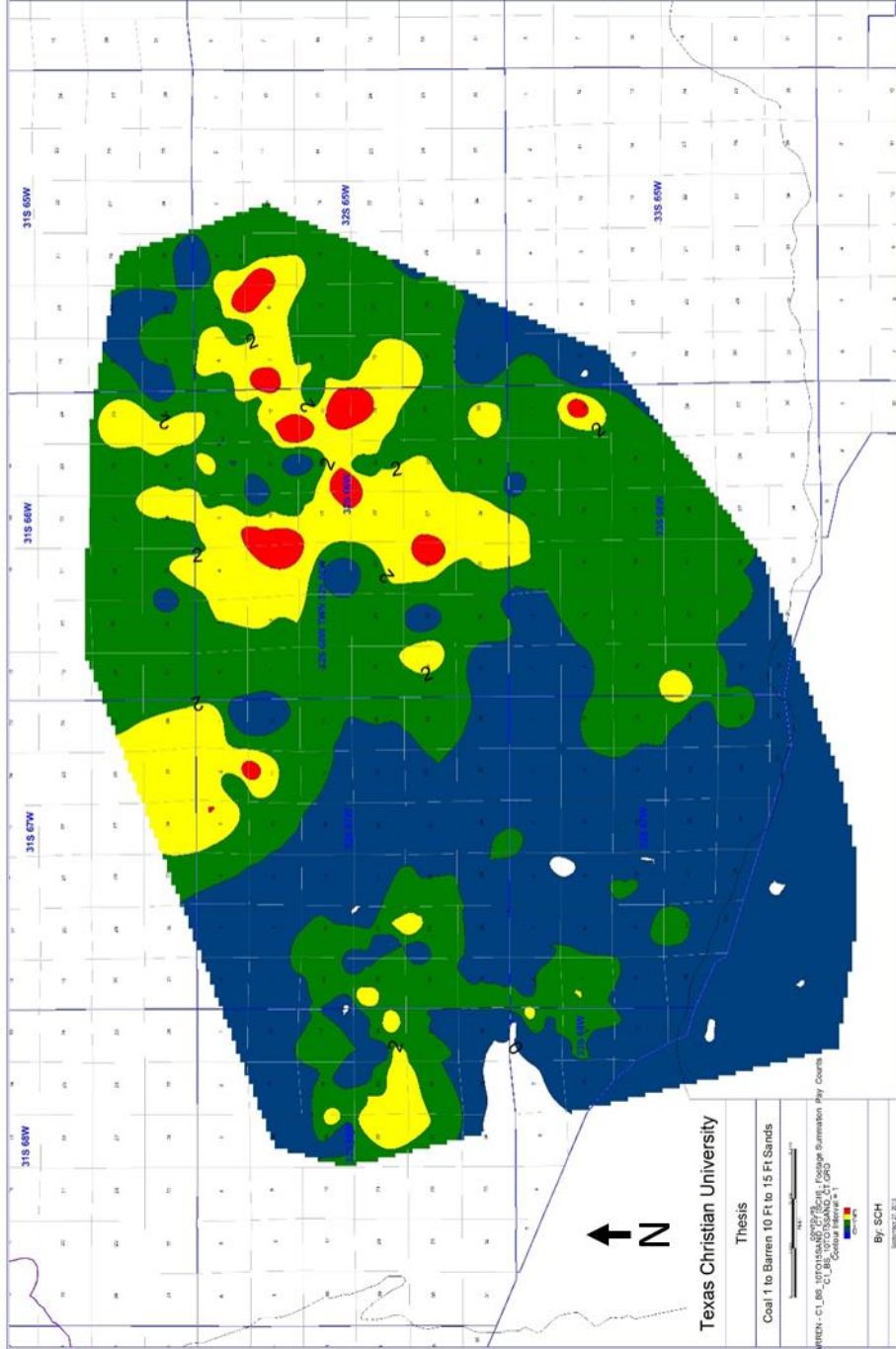
Figure 31: Frequency map of the number of sand intervals between 10ft and 15ft thick between coal x and the top of the barren series. Contours are on a 1 frequency interval and range from 0 to 3 sandstones. Green color fill on the map indicates areas where there is a lower count of sand intervals. Reds and oranges indicate areas where there is a higher concentration of sand intervals.

Chapter 4: Discussion

Raton Conglomerate:

The Raton conglomerate was deposited by an alluvial fan as suggested by Pillmore and Flores (1987) and Osterhout (2014). In core and outcrop, the Raton conglomerate comprises pebble to cobble sized grains suggesting a higher energy depositional system. This is shown in the well logs with low gamma ray readings that can be correlated throughout the study area. The isopach map for the Raton conglomerate (Figure 14) can be interpreted as a fan system. The map displays a thick mound on the western flank of the study area and thins to the north, east, and southeast in a radial fashion. The fan apex is interpreted to be the prominent thick on the eastern margin and therefore was the area of entry for the fan as it dispersed down dip to the east. Zircon data published by Bush (2016) suggests that the source of the Raton Conglomerate was the Sangre de Cristos to the west of the Raton Basin. The isopach map supports this as the depocenter in the west suggests that the alluvial fan originated from the Sangre de Cristo Mountains on the western flank of the basin.

Lower Coal zone:

The lower coal zone isopach map (Figure 15) coupled with the sandstone (Figure 17) and coal (Figure 16) percentage maps indicate that there were two channel belts running southwest to north east though the study area. The sandstones were distributed throughout the basin as a lattice of thin channel belts. Areas with higher percentages of sandstone were channel belts that persisted over longer durations and/or were larger in extent. The channel belts are very apparent on the lower coal zone sandstone percentage map, which displays two larger trends extending from the western side of the study area to the eastern side. Furthermore, trends from the 1 to 5 ft sandstone frequency

map seem to follow the same trends as the sandstone percentage map and also display a channel like geometry (Figures 18 and 32). Channel belts from the 1 to 5 ft interval do not capture the northern channel trend but are distinctive in the southern channel belt trend. When compared to the Raton conglomerate isopach map, the northern channel belt trend of the lower coal zone is just off the edge of the Raton conglomerate thick. This suggests that there is a common point of entry between the Raton conglomerate and the lower coal zone fluvial system. The spatial distribution between the apex of the Raton conglomerate fan and the lower coal zone northern channel belt trend suggests that there is some inherited control on the channels from the previous depositional event. The channels, however, enter on the flanks of the thick in the Raton conglomerate. This suggests a piling at the fan apex guided streams around this thick. The southern channel belt does not correspond to any trends within the Raton conglomerate and appears to be a separate channel system entering the basin. Areas with higher coal percentages also form a complex lattice and locally are inverse of those areas with higher sandstone percentages (Figure 16 and 17). This is likely because these channel belts are supplying enough sediment into the system to deter the formation of peat, or are forming areas of minimal compaction.
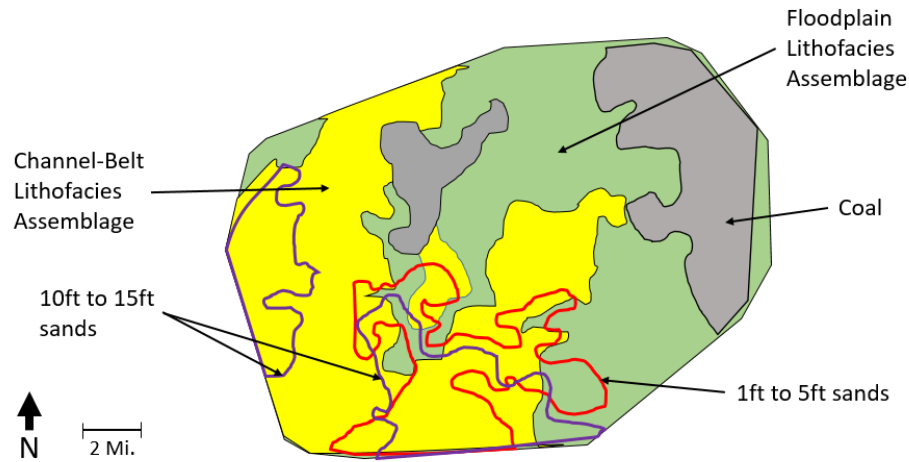
Lower Coal Zone

Figure 32: A map showing the interaction between the different lithofacies assemblages and sandstone thickness intervals for the lower coal zone.

The areas where the sandstone percentage is low and the mudstone and coal percentages are high are likely areas where the floodplain and lake lithofacies assemblages dominate (Figure 32). These assemblages are better developed down depositional dip on the eastern side of the basin. Sandstones with a thickness between 1 and 5 ft are predominantly located in the southern portion of the basin and create a channel form shape (Figure 18). Sandstones with these thicknesses likely represent both the splay lithofacies as well as the channel lithofacies within the lower coal zone. Sandstones between 5 and 10 ft (Figure 19) thick are predominantly located in the southern portion of the study area. Sandstones of this magnitude are areas where the channel lithofacies assemblage and valleys are prominent. The distribution of channels and flood basin deposits suggest a complex and shifting lattice of channels with large lake and swamp areas between. Channels are diminished in prominence down dip with some persistence of channel trends locally. The location of protracted channel trends is likely related to the location of channel entry points into the basin.

66

The distribution of lithofacies assemblages agrees with Harrison's (2018) interpretation of the lower coal zone having been deposited in a channel-floodplain depositional environment. The floodplain lithofacies assemblage dominates the lower coal zone interval. Within the lower coal zone, the coals are typically thin (less than 2 ft) and discontinuous. This suggests coals were deposited within the floodplain lakes and seldom in larger, more stable lacustrine systems. Additionally, there are intervals of carbonaceous mudstone present within the lower coal zone. Seasonal, smaller floodplain lakes in the low-lying areas adjacent to fluvial channels account for the presence of the thinner coals.
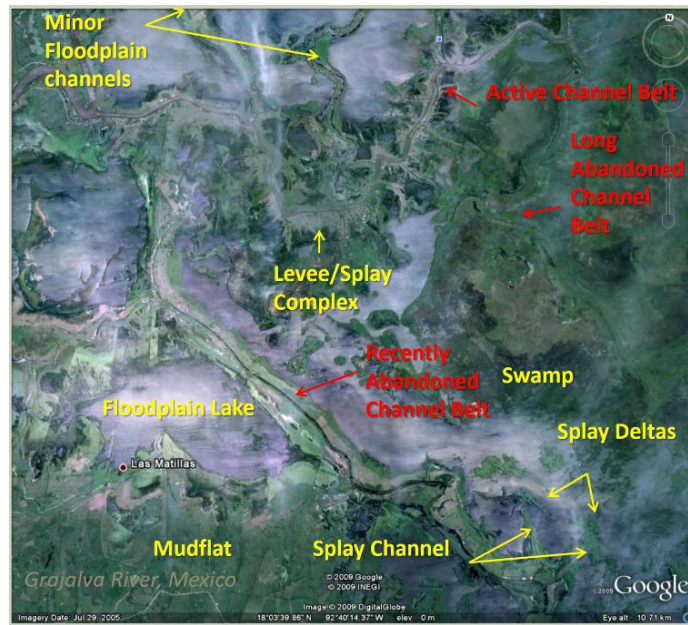

Figure 33: The Grijalva river system in Tabasco, Mexico with geomorphological features (Hull 2016; Harrison, 2018).

A modern day analog of this system is the Grijalva River system in Tabasco, Mexico (Figure 33) (Harrison, 2018). The Grijalva is a high-accommodation, poorly drained floodplain basin containing floodplain lakes, mudflats, and propagating tie channels cutting through lakes (Hull, 2016; Harrison, 2018). The larger floodplain lakes tend to remain constant, while smaller lakes can be ephemeral, producing simple, rooted soils (Stoner, 2010; Harrison, 2018). Channel

belts generally narrow and bifurcate down dip. The Grijalvas' water table is highly variable. Large

swathes of relatively dry floodplain and abandoned channels are frequently flooded, as are the

smaller floodplain lakes (Harrison, 2018).

Barren Series:

The informal barren series member of the Raton Formation displays a fan shaped

depositional system (Figure 34). The barren series isopach map shows that the member is thickest

in the southwestern portion of the study area. From the southwest, the barren series interval thins

in a radial pattern, ultimately reaching its thinnest point in the eastern portion of the study area

(Figure 20). A higher concentration of sandstones occurs in the southern portion of the study area,

whereas there is a higher percentage of coal and mudstone in the northern portion of the study area

(Figures 21 and Figure 22). The spatial distribution of the sandstone, coal, and mudstone suggest

that the fan is sourced from the south and coal deposition occurred down dip at the toe of the fan.

This concurs with the classic depositional definition of a fan in that coarser grained sediments
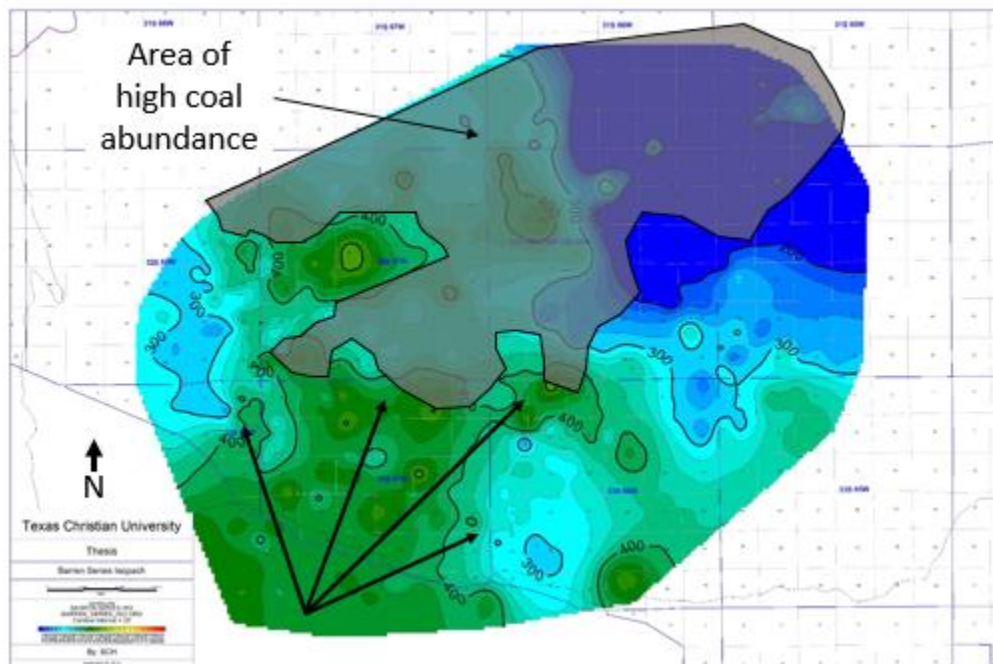

**Figure 34: The barren series isopach map displaying the radial thinning trends overlain
by the area of high coal abundance (gray polygon).**

occur closer to the source and finer grained sediments and coals are found in the distal, thinner portions of the fan (Figure 34).

Sandstone thicknesses and their distribution provides insights on the depositional environment. The 1 to 5 ft thick sandstones (Figure 23) are found throughout the study area but are mainly concentrated in the western half of the basin. These sandstones likely represent small channel and potentially splay complexes noted be Horner (2016) (Figure 35). These sandstones have a clear dispersive pattern from at least two points on the south boundary of the study area. The 10 to 15 ft thick sandstones occur in the western and southern portion of the study area (Figure 24). These sandstones may form a channel like or geometry collectively or a lobate geometry individually. It is likely that sandstones of this thickness are valley fills that are present within the barren series interval. It is also possible that these are the larger terminal splay complexes that Horner (2016) described in the Lower Valdez outcrop (Figure 35). The 15 to 20 ft sandstone packages (Figure 25) occur in the central and southern portion of the study area and likely represent
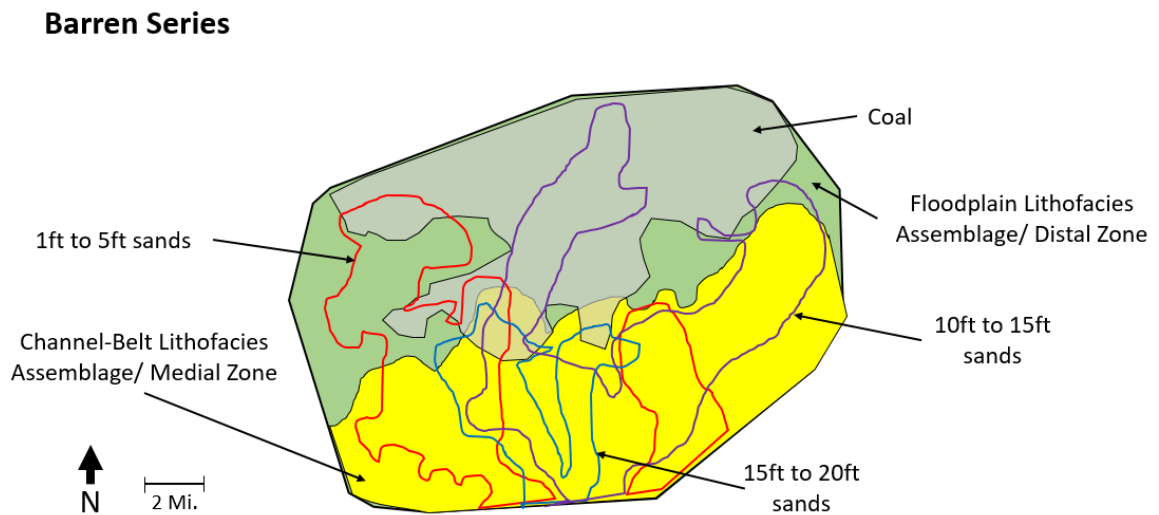

Figure 35: A map showing the interaction between the different lithofacies assemblages and sandstone thickness intervals for the barren series.

the valley-fill lithofacies super-assemblage as seen at the Exit 6 outcrop described by Horner (2016) (Figure 35).

The barren series isopach map (Figure 20) and sandstone percentages (Figure 22) indicate a sediment source coming from the south. This is in agreement with the zircon study conducted by Bush et al. (2016) which concluded that the barren series was sourced by exhumation of the Sangre de Cristos during the early Paleogene. Furthermore, leaf assemblage studies by Wolfe and Upchurch (1987) indicate a major increase in precipitation at the K-Pg boundary within the Raton Basin. In addition, at the time of the K-Pg event, vegetation was annihilated drastically changing erosional and floral systems temporarily (Wolfe and Upchurch, 1987; Pillmore and Fleming, 1990; Pillmore et. al., 1999). The increase in precipitation coupled with the exhumation of the Sangre de Cristo Mountains and lack of vegetation pushed more sediments into the basin, preventing significant coal deposition within the barren series. It is the lack of economic coals that gives the barren series gets its name.

The fan-shaped geometry of the barren series isopach map as well as the distribution of the lithofacies assemblages indicate a distributive fluvial system deposited the barren series interval. A Distributive Fluvial System will typically have a higher abundance of sandstones and channels in the proximal zone. As sediment moves down dip into the medial zone, floodplain mudstones begin to form, and overbank deposits become more prevalent. Terminal Splay sandstones, coals, and a higher abundance of mudstones comprise the distal zone of the Distributive Fluvial System (Nichols and Fisher, 2007; Hartley et al., 2010). The higher abundance of sandstones in the southern portion of the study area (Figure 32) that transitions into the higher abundance of coal (Figure 31) and mudstone in the northern part of the area indicates the barren series was deposited in the medial to distal zones of the DFS model (Figures 7 and 8). Furthermore, the lack of sandstone

presence (Figure 22) in the southwestern portion of the study area indicates that the head of the DFS fan is not present in this area. Coals found within the distal portion of the barren series are discontinuous, thin (less than 1 ft), and are not correlatable. This is likely because the coals found within the barren series were deposited in the distal DFS below the spring line (Figure 7) during periods of time in which the floodplains became inundated with water allowing for the preservation of peat. Furthermore, Horner (2016) identified both individual terminal splays and terminal splay complexes in outcrops of the barren series interval. Both Harrison (2018) and Horner (2016) mapped multiple channel forms in outcrop that were deposited under unconfined flow conditions. Unconfined flow is characteristic of the medial and distal portions of a DFS (Nichols and Fisher, 2007). It is also common for DFS systems to be incised by buffer valleys (Figures 24 and 25) because of climatic changes in the headwaters (Holbrook, 2006; Nichols and Fisher, 2007; and Hartley et al., 2010).

The sandstone interval thickness maps suggest that larger river and valley systems that entered the basin from the south skirted the higher topography of the fan apex. This suggests that these are two different systems and the higher topography of the fan forced the larger channels into a basin axial orientation.

Upper Coal Zone:

Coals found within the upper coal zone suggest a backstepping over the barren series. Coals within the upper coal zone, labeled in gray, appear to onlap the barren series in the eastern portion of the basin before ultimately overlapping the barren series in the west (Figures 12 and 36). This was likely caused by the sloped topography of the DFS that was buried as the upper coal zone began to aggrade. This aggradation began as the siliciclastic sediment supply began to decrease, eventually allowing the upper coal zone to onlap the barren series.
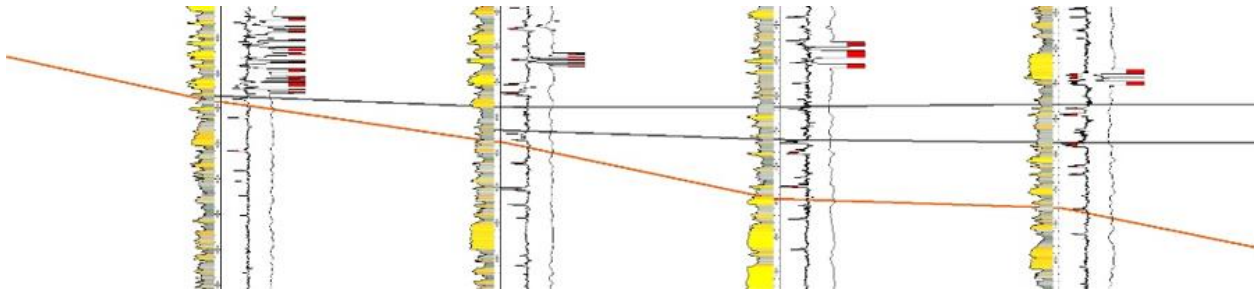
Figure 36: A cross section showing the onlap of the upper coal zone coals (gray) over the top of the barren series interval (red).

The upper coal zone was sourced from the southwestern portion of the study area and marked a return to the channel-floodplain depositional environment similar to the lower coal zone. The 1ft to 5ft sandstone interval map shows that sandstones of this thickness are predominantly located in the eastern portion of the study area (Figure 29). Sandstones of this thickness likely represent the presence of small channels and terminal splay complexes by the backstepping DFS over the barren series. This indicates that the eastern flank of the study area is more distal from the source. The 5 to 10 ft sandstones occur in the southwestern portion of the study area and likely represent channel belts (Figure 40). These larger channel belts coupled with the higher concentration of sandstones in the southern half of the study area suggests that the sediment supply was sourced from the south (Figure 37). The 5 to 10 ft sandstones (Figure 30) of the upper coal zone are concentrated in the southern portion of the study area, where the upper coal zone is thinnest. This trend appears to follow the 1 to 5 ft sandstones of the barren series (Figure 23) almost exactly, suggesting that the upper coal zone inherited this basin axial channel entry point from the barren series. The higher topography of the barren series fan apex may have influenced these channel trends. The 10 to 15 ft sands located in the eastern half of the basin (Figure 37) suggest that valley fills occasionally cut through and terminated within the upper coal zone. Evidence of this is clearly indicated in work by Harrison (2018) at the King Coal outcrop. This outcrop displays

72

a large valley fill cutting through lacustrine and floodplain sediments overlying one of the major coals of the basin.
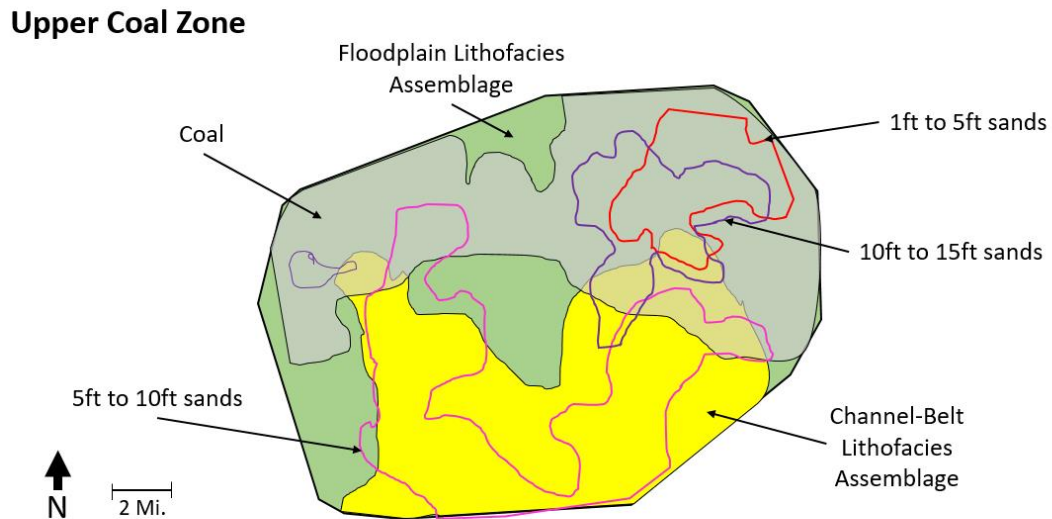

Figure 37: A map showing the interaction between the different lithofacies assemblages and sandstone thickness intervals for the upper coal zone.

Unlike the lower coal zone, the upper coal zone is prone to transitions between the channel-floodplain depositional system and fluvial-lacustrine depositional system (Harrison, 2018). This is driven by changes in groundwater level. When the ground water table is low, deposition occurs within the trunk channel and in adjacent well-drained floodplains (rooted floodplain fines and paleosols). Splay events and splay channels are frequent, depositing the sand sheet element of the floodplain assemblage (Harrison, 2018). As the groundwater table rises, the floodplain becomes inundated with water creating the laminated mudstone (Flm), carbonaceous mudstone (Fcm), and thin sand (blow out wing) lithofacies associated with the lacustrine assemblage (Harrison, 2018). Peat is preserved during optimal episodes of lake evolution when the system experienced minimal sediment influx and preserved organic materials (Harrison, 2018). During these time periods thick,

laterally extensive coals were deposited within the upper coal zone. These coals can be correlated for tens of miles throughout the Raton Basin (Osterhout, 2014; Roy Pillmore, Personal Comm. 2018). An example of this is coal x (Figure 12), which is correlatable throughout the study area and represents a period of time when the Raton Basin was inundated with water and the lacustrine assemblage was being deposited. Work from Harrison (2018) suggests that the lake and floodplain dominated systems alternate, so the sandstone channels and the coal-forming lakes are not always contemporaneous.

Neither the lake nor the floodplain systems have the terminal splay complexes or the clear apical thickness trend of the barren series. They still have a general distributive pattern, but this pattern is more reflective of dispersion of channels into a generally low, swampy or floodplain system. Thicker channels that entered along the basin axis from the south commonly bifurcate or splay into thinner sandstones toward the north. These deposits were distributive into the basin, but formed low-sloping floodplain and fluvial lacustrine and dominantly axial distributive systems, instead of the more robust DFS typical the barren series that drained the mountains to the west. The persistent topography of the barren DFS likely turned rivers toward the basin axis as the upper coal zone member onlapped the older barren series topography from the east.
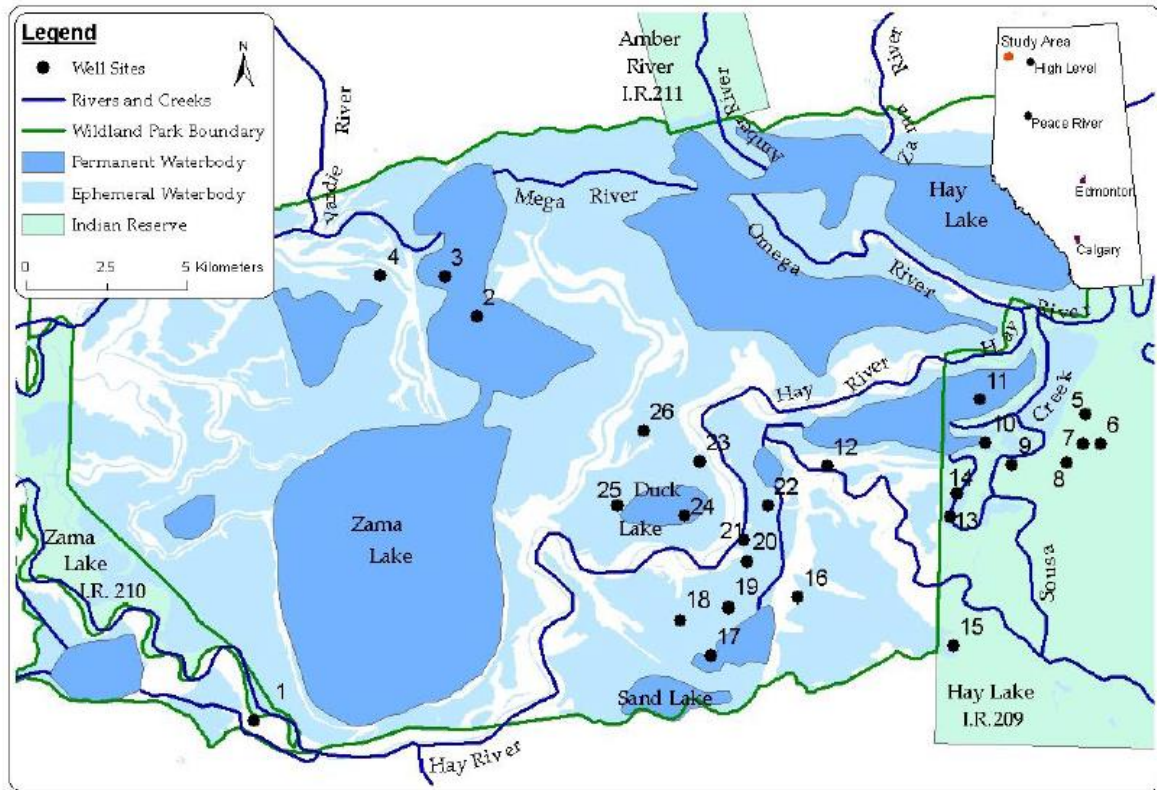
Figure 38: Hay-Zama Lake System. The dark blue lines represent active channels, regular blue represents lakes, and light blue represents ephemeral lakes. White areas represent levees and channel deposits (Wright, 2005; Harrison, 2018).

Modern analogs suggested by Harrison (2018) for the fluvio-lacustrine and thick coal deposition within the Raton Basin are the Hay-Zama Lake of Alberta, Canada, and the Okefenokee Swamp of northern Georgia (Harrison 2018). Hay-Zama Lake (Figure 38) is a group of fresh-water lakes with varying water depths. During the wet season, the lakes expand and often merge to form one larger lake (Wight, 2005; Huling, 2014; Harrison, 2018). The long lasting shallow lake basin with discrete channels is similar to the fluvio-lacustrine environment of the Raton Formation (Harrison 2018). The Okefenokee Swamp is an inundated, peat-forming swampland located in southeastern Georgia. Standing water with floating marsh grasslands composed of predominantly cypress trees comprise the swampland (Cohen, 1974; Harrison 2018). Two prominent fluvial channels within the Okefenokee cut through and drain the swamp.

The Okefenokee Swamp is a peat producing swamp with peat deposits up to 15 ft thick (Cohen, 1974; Harrison 2018). Both Hay-Zama and the Okefenokee fit certain aspects of the fluvio-lacustrine depositional system of the upper coal zone, but neither are a perfect analog (Harrison, 2018).

Paleogeography:

The Raton conglomerate was deposited by an alluvial fan sourced from the western flank of the Raton Basin. The Raton conglomerate thickness trends suggest that the source of sediment for the alluvial fan was the western flank of the Raton Basin (Figure 39). Zircon dating from Bush et. al., (2016) suggests that the Raton conglomerate is composed of recycled Permian sediments from west of the Raton Basin eroded during the initial exhumation of the Laramide basement uplifts.
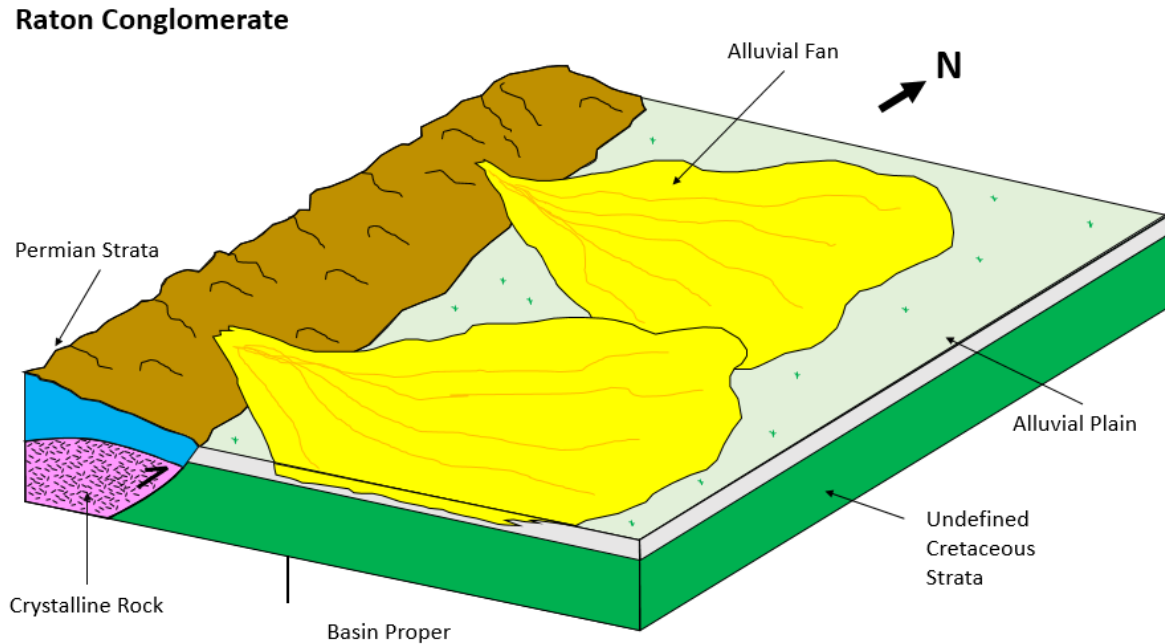

Figure 39: A paleogeographic cartoon of the Raton Basin during deposition of the Raton conglomerate.

The lower coal zone was deposited within a channel-floodplain, and like the Raton conglomerate, was sourced from the western flank of the Raton Basin (Figure 40). The lower coal zone isopach map shows an overall thinning trend toward the eastern flank of the study area. This, coupled with trend of decreasing sandstones in the eastern side of the study, support the idea of a western source. Much like the Raton conglomerate, zircon data from Bush et al. (2016) suggest that the sediment supply was derived from the initial unroofing of Laramide block uplifts.

Lower Coal Zone
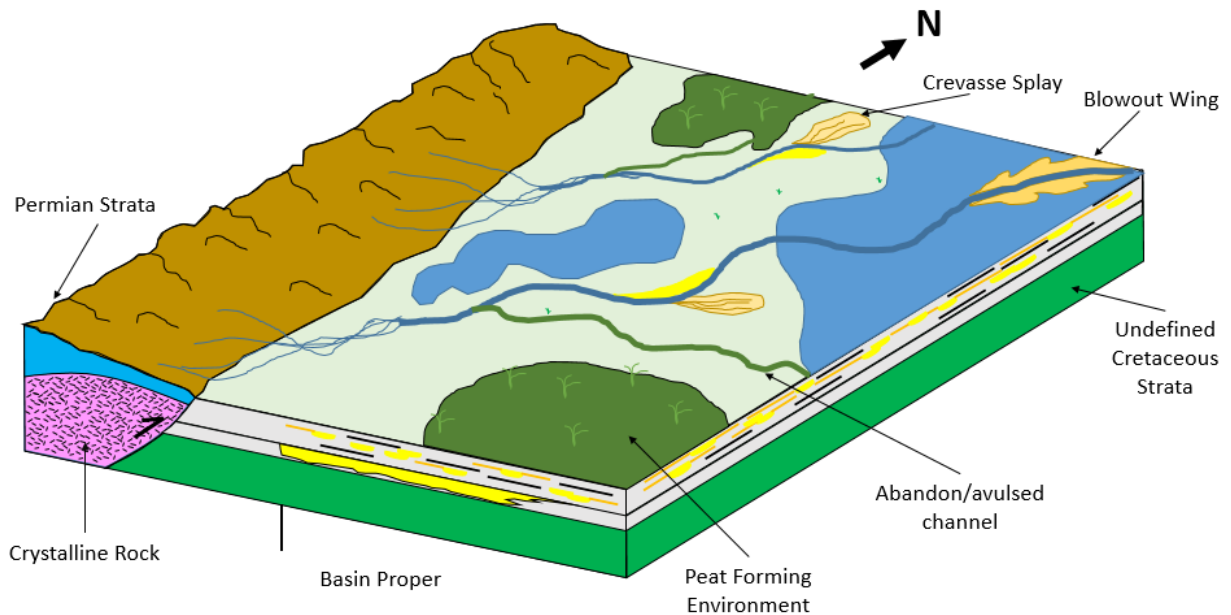
Figure 40: A paleogeographic model of the Raton Basin during deposition of the lower coal zone.

The barren series was deposited by a distributive fluvial system that was sourced from the southwest (Figure 41). The barrens series isopach map displays a fan shape with the thickest section in the southwestern portion of the study area. From this thick interval, the barren series thins in a radial fashion, with the thinnest portion found in the eastern flank of the study area. Zircon data from Bush et al. (2016) suggest that sediment was sourced from the Proterozoic

basement rocks that comprise the Sangre de Cristos to the west. During this time, the uplift of the Culebra Range of the Sangre de Cristos produced a shift in source from the west to the southwest.

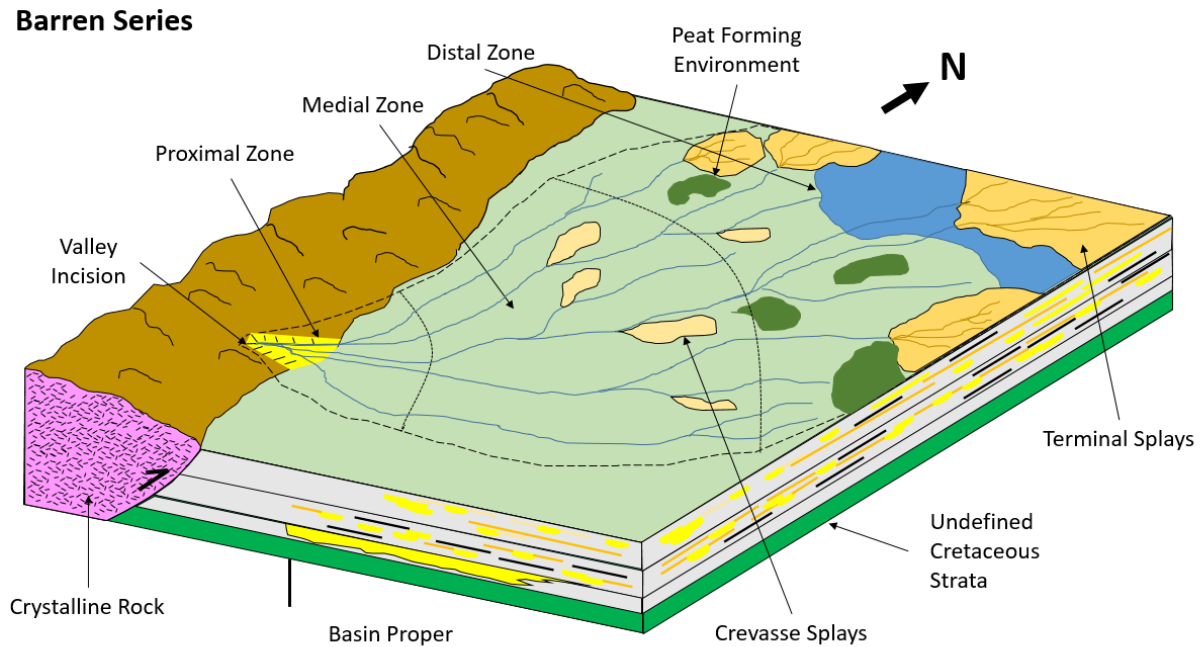**Figure 41: A paleogeographic model of the Raton Basin during deposition of the barren series.**

The upper coal zone was deposited within fluvio-lacustrine and channel-floodplain depositional environments, and was sourced from the south (Figure 42). Channel sandstones identified on the 5 ft to 10 ft and 15 ft to 20 ft interval maps, coupled with the high concentration of sandstones in the southern portion of the study area, support the hypothesis of a southern source. Much like the barren series, zircon data from Bush et al. (2016) suggest that the sediment source was the Culebra Range of the Sangre de Cristos. Unlike the other intervals within the Raton Formation, the upper coal zone regularly shifted from a channel-floodplain environment (Figure 42A) to a peat-forming, fluvio-lacustrine environment (Figure 42B). The latter environment is marked by the presence of laterally continuous, basin-wide coals.
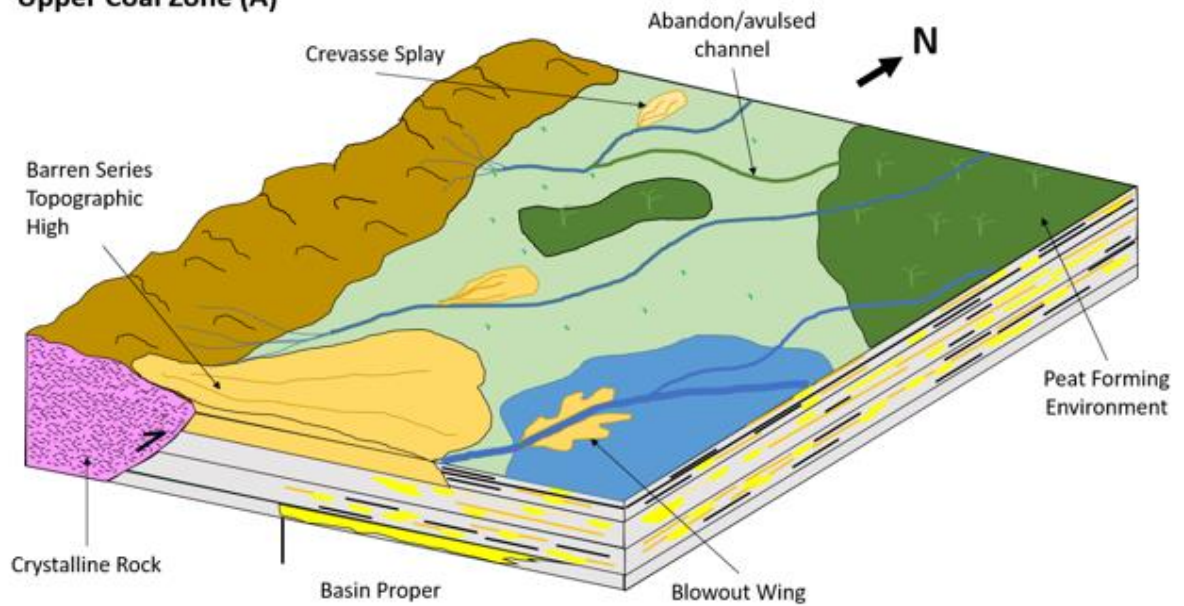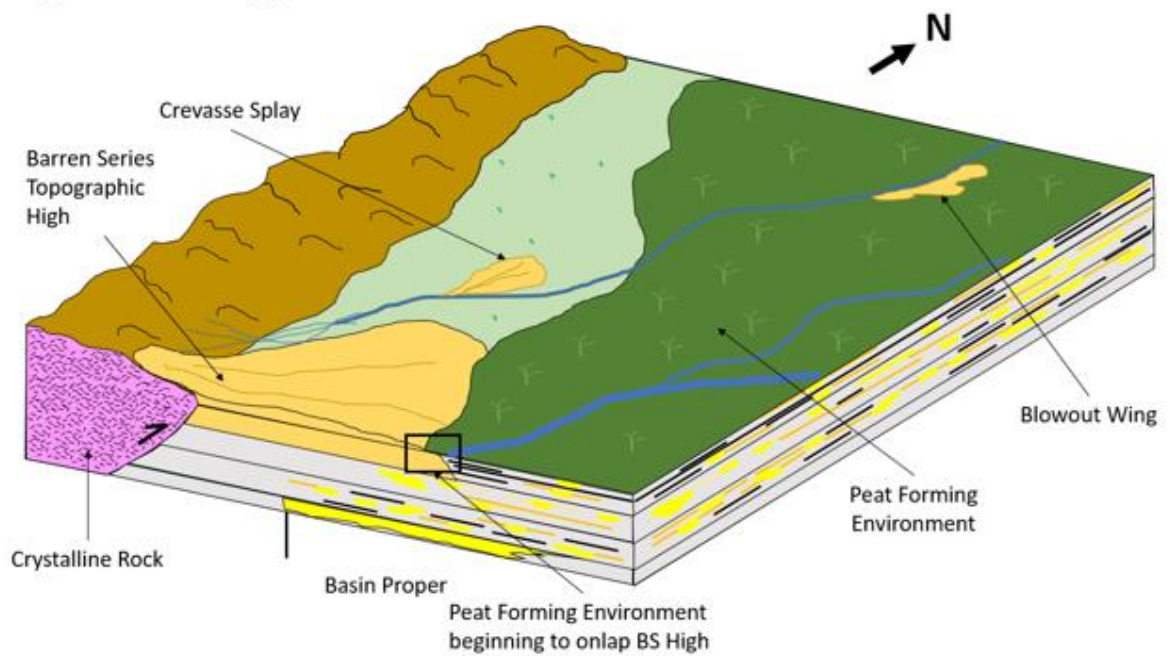
Figure 42: Paleogeographic models of the Raton Basin during deposition of the upper coal zone. Upper coal zone (A) represents a time a channel-floodplain environment. Upper coal zone (B) represents a fluvio-lacustrine environment.

Industry Implications:

Economic coal bed methane targets are common in the Raton Formation but concentrated in the northeastern part of the study area and in the lower and upper coal zones. Coal bed methane wells target coals with a minimum thickness of 0.5 meters (Osterhout, 2014). Wells within the Raton Basin complete between 6-20 different coals between the Vermejo and Raton formations (Osterhout, 2014). Coal percentage maps (Figure 16, 21, and 28) indicate a higher abundance of coals in the northern portion of the study area. Coals within the lower coal zone are typically discontinuous, but reach thicknesses of over a meter (Harrison, 2018) (Figure 16). The barren series derives its name from the fact that it does not contain economic coals. This holds true for coal bed methane exploration. Coal beds within the barren series are found predominantly in the northern portion of the study area, but are thin (< 0.5 m) and discontinuous (Figure 21). Coals within the upper coal zone are thick ($\geq$ 2.5 m) and can extend tens of miles. Coals are highly abundant within this interval allowing for multiple targets per coal bed methane well (Figure 28). These coals are wider dispersed and more abundant in the eastern part of the study area.

The Raton Formation also has potential for conventional gas plays within channel sand trends and terminal splay complexes. Channel sands are mainly located within the channel fairways of the lower and upper coal zones. Within the lower coal zone, conventional targets will be predominantly located within the two sand rich trends running southwest-northeast (Figure 17). Channels range in thickness from 1-10 feet thick rarely exceeding this size (Figure 18 and 19). The upper coal zone's main channel fairway is located in the eastern portion of the study area. Channels range in size from 1-10 feet (Figure 27, 29, and 30). Valleys are also present within this channel fairway ranging in size from 10- 20 feet in thickness (Figure 31). Fluvial sands within the Raton Basin are typically encased in impermeable floodplain and lacustrine mudstones acting as a seal

for the potential reservoir. Coals surrounding these fluvial sands are the probable source of the gas. Horner (2016) and Harrison (2018) suggests that terminal splays, crevasse splays, and blow out wings have the potential to increase the connectivity of the reservoir sands. These laterally extensive sands have the potential to act as hydrocarbon conduits in an otherwise muddy unit. Blowout wings are common in lacustrine strata throughout the upper and lower coal zones. Terminal splay complexes are restricted to the barren series.

CHAPTER 5: Conclusions

1) The Raton conglomerate of the Raton Formation records an alluvial fan sourced from the Sangre de Cristo Mountains to the west.

2) The lower coal zone of the Raton Formation formed in a channel-floodplain depositional system with feeder channels originating predominantly from an axial system to the south. Antecedent topography created by the deposition Raton conglomerate likely influenced the river patterns of the overlying lower coal zone. The coaly intervals of the lower coal zone are discrete, do not correlate over long distances, and likely formed in floodplain lakes and swamps adjacent to a complex lattice of channels.

3) The barren series records a Distributive Fluvial System radiating from the Sangre de Cristo Mountains into the southwestern portion of the study area. Coal deposits are thin, uncommon, and formed in the distal swamps of the DFS. The barren series is also the only interval where the terminal splay lithofacies has been recorded. An axial fluvial system entered the study area from the south and was controlled by the higher topography of the DFS fan to the southwest.

4) The upper coal zone formed in both channel-floodplain and fluvio-lacustrine systems. The upper coal zone aggraded as siliciclastic sediment supply waned during the deposition of the barren series, producing an onlapping relationship between the two intervals. Laterally extensive coals, like coal x, were deposited when the basin was dominated by fluvio-lacustrine environments. Sandstone percentage and frequency maps indicate that siliciclastic sediments were sourced mostly from an axial system to the south that was inherited from the axial fluvial system of the barren series interval. The axial system of the upper coal zone is

controlled by the antecedent topography of the barren series DFS fan located in the southwestern portion of the study area.

5) The transition between the channel floodplain depositional system of the lower coal zone and distributive fluvial system of the barren series occurred from a culmination of factors including uplift and exhumation of the Sangre de Cristos, mass extinction of vegetation because of the K-Pg extinction event, and an increase in rainfall event causing a higher rate of erosion.

.

References:

Baltz, E. H. (1965). Stratigraphy and History of Raton Basin and Notes on San Luis Basin, Colorado-New Mexico. *Bulletin of the American Association of Petroleum Geologists,* v. 49(11), pp. 2041-2075. doi:http://dx.doi.org/10.1306/A6633882-16C0-11D7-8645000102C1865D

Bohacs, K. and Suter, J. (1997). Sequence stratigraphic distribution of coaly rocks: fundamental controls and paralic examples. *Bulletin of the American Association of Petroleum Geologists*, v. 81(10), pp. 1612-1639.

Bush, M. A., Horton, B. K., Murphy, M. A., & Stockli, D. F. (2016). Detrital record of initial basement exhumation along the Laramide deformation front, southern Rocky Mountains. *Tectonics*, v. 35(9), pp. 2117-2130.

Clarke, P. R., Cornelius, C., & Turner, P. (2002). *Alluvial Processes and Sansbody Architecture in the Raton Basin*. Paper presented at the AAPG Rocky Mountain Section, Laramie, Wyoming.

Clarke, P., Cornelius, C., & Turner, P. (2004). *A Refined Lithostratigraphy for the Raton Formation: Implications for Alluvial Heterogeneity, Coal-Forming Environments and Coal Bed Distribution-Raton Basin*. Paper presented at the 2004 Denver Annual Meeting.

Cohen, A. D. (1974). Petrography and paleoecology of Holocene peats from the Okefenokee swamp-marsh complex of Georgia. *Journal of Sedimentary Research*, v. 44(3), pp. 716-726.

Diessel, C.F.K., 1992. Coal-Bearing Depositional Systems: Springer, Verlag, Berlin. pp. 721

Fisher, J.A., Krapf, C.B.E., Lang, S.C., Nichols, G.J. and Payenberg, T.H.D. (2008) Sedimentology and Architecture of the Douglas Creek Terminal Splay, Lake Eyre, central Australia. *Sedimentology*, v. 55, 1915–1930.

Flores, R. M. (1984). Comparative Analysis of Coal Accumulation in Cretaceous Alluvial Deposits, Southern United States Rocky Mountain Basins. *Memoir - Canadian Society of Petroleum Geologists,* v. 9, pp. 373-385.

Flores, R. M. (1985). Coal Deposits in Cretaceous and Tertiary Fluvial Systems of the Rocky Mountain Region. *U. S. Geological Survey Professional Paper*, pp. 1-50.

Flores, R. M. (1987). Sedimentology of Upper Cretaceous and Tertiary Siliciclastics and Coals in the Raton Basin, New Mexico and Colorado: 38th Field Conference, Northeastern New Mexico, *New Mexico Geological Society Guidebook*, pp. 255-264.

Flores, R. M., & Bader, L. R. (1999). A Summary of Tertiary Coal Resources of the Raton Basin, Colorado and New Mexico. *U. S. Geological Survey Professional Paper*.

Flores, R. M., & Pillmore, C. L. (1987). Tectonic Control on Alluvial Paleoarchitecture of the Cretaceous and Tertiary Raton Basin, Colorado and New Mexico. *Special Publication - Society of Economic Paleontologists and Mineralogists,* v. 39, pp. 311-320.

Graham, J.R. (1983). Analysis of the Upper Devonian Munster Basin, an Example of a Fluvial Distributary System. In: Collinson, J.D., Lewin, J. (Eds.), Modern and Ancient Fluvial Systems, *Special Publication- International Association of Sedimentologists*, v. 6, pp. 473-484.

Hartley, A. J., Weissmann, G. S., Nichols, G. J., & Warwick, G. L. (2010). Large Distributive Fluvial Systems: Characteristics, Distribution, and Controls on Development. *Journal of Sedimentary Research,* v. 80(2), pp.167-183.

Harrison, R. I. (2018). Depostitional Enviroments of Cretaceous- Paleogne Coal Beds and Surrounding Strata Within The Raton Basin Of Colorado and New Mexico, USA. *Texas Christian University* (Master's Thesis).

Hirst, J.P.P. (1991). Variations in Alluvial Architecture Across the Oligo-Miocene Huesca Fluvial System, Ebro Basin, Spain. *SEPM Special Publication,* v. 3, pp. 111-121.

Hoffman, G. K., & Brister, B. S. (2003). New Mexico's Raton Basin Coalbed Methane Play. *New Mexico Geology,* v. 25(4), pp. 95-110.

Holbrook, J. M., Scott, R.W., & Oboh-Ikuenobe, F.E. (2006). Base-Level Buffers and Buttresses: A Model for Upstream Versus Downstream Control on Fluvial Geometry and Architecture Within Sequences. *Journal of Sedimentary Research*, v. 76(1), pp. 162-174.

Horner, R. J. (2016). Facies Characterization and Architectural Context of Terminal Splay Sandstones Beds in the Cretaceous-Paleocene Raton Formation, Colorado. Texas Christian University (Master's Thesis).

Huling, G. A. (2014). Evidence for clustering of delta-lobe reservoirs within fluvio-lacustrine systems, Jurassic Kayenta Formation, Utah [electronic resource]. UMI thesis.

Hull, M. (2016), A modern reservoir analogue for a poorly drained "high accommodation" fluvial system: Sedimentary processes, architecture, and reservoir connectivity of the Grijalva system, Tabasco State, Mexico, The University of Texas at Arlington, (Ph.D Thesis)

Johnson, R. B., Dixon, G. H., & Wanek, A. A. (1956). Late Cretaceous and Tertiary Stratigraphy of the Raton Basin of New Mexico and Colorado. Socorro, New Mexico, United States (USA): *N. M. Geol.* Soc., Socorro, New Mexico. pp. 122-133

Johnson, R. B., & Wood Jr, G. H. (1956). Stratigraphy of Upper Cretaceous and Tertiary Rocks of Raton Basin, Colorado and New Mexico. *AAPG Bulletin,* v. 40(4), pp. 707-721.

Johnson, R. C., & Finn, T. M. (2001). Potential for a Basin-Centered Gas Accumulation in the Raton Basin, Colorado and New Mexico. *U. S. Geological Survey Bulletin*. pp. 1-14.

Lee, W. T., & Knowlton, F. H. (1917). Geology and paleontology of the Raton Mesa and other regions; Colorado and New Mexico U. S. *Geological Survey Professional Paper*. Reston, VA, United States (USA): U. S. Geological Survey, Reston, VA.

MacCarthy, I.A.J. (1990). Alluvial Sedimentation Patterns in the Munster Basin, Ireland. *Sedimentology,* v. 37, pp. 685-712.

McCabe, P. J., & Parrish, J. T. (1992). Tectonic and climatic controls on the distribution and quality of Cretaceous coals. *Geological Society of America Special Papers*, v. 267, pp. 1-16.

Miall, A. D. (1996). *The geology of fluvial deposits: sedimentary facies, basin analysis, and petroleum geology*: Springer, Verlag, Berlin. pp. 581.

Nichols, G.J., and Fisher, J.A. (2007). Processes, Facies and Architecture of Fluvial Distributary System Deposits. *Sedimentary Geology,* v. 195, pp. 75-90.

Norwest Corporation (2010). *Central Raton Basin Groundwater Modeling Project*.

Orth, C. J., Gilmore, J. S., Knight, J. D., Pillmore, C. L., Tschudy, R. H., & Fassett, J. E. (1981). An Iridium Abundance Anomaly at the Palynological Cretaceous-Tertiary Boundary in Northern New Mexico. *Science,* v. 214(4527), pp. 1341-1343.

Osterhout, S. L., Rothkopf, B. W., & Soetrisno, H. (2014). Raton Basin: Raton Basin Coal Bed Methane Gas Field, Colorado and New Mexico. *Oil and Gas Fields of Colorado,* pp. 267-292.

Pillmore, C. L. (1976). Commercial Coal Beds of the Raton Coal Field, Colfax County, New Mexico. *Guidebook - New Mexico Geological Society,* v. 27, pp. 227-247.

Pillmore, C. L., & Flores, R. M. (1987). Stratigraphy and Depositional Environments of the Cretaceous-Tertiary Boundary Clay and Associated Rocks, Raton Basin, New Mexico and Colorado. *Geological Society of America Special Papers,* v. 209, pp. 111-130.

Pillmore, C. L., & Flores, R. M. (1990). Cretaceous and Paleocene Rocks of the Raton Basin, New Mexico and Colorado; Stratigraphic-Environmental Framework. *Guidebook - New Mexico Geological Society,* v. 41, pp. 333-336.

Pillmore, C., Nichols, D., & Fleming, R. (1999). Field guide to the continental Cretaceous–Tertiary boundary in the Raton Basin, Colorado and New Mexico. *Colorado and Adjacent Areas,* v. 1, pp. 135-155.

Pillmore, C. L., & Maberry, J. O. (1976). Depositional environments and trace fossils of the Trinidad Sandstone, southern Raton basin, New Mexico in Guidebook of Vermejo Park, northeastern New Mexico: *New Mexico Geological Society Guidebook*. Paper presented at the 27th Field Conference.

Sadler, S.P., and Kelly, S.B. (1993). Fluvial Processes and Cyclicity in Terminal Fan Deposits: an Example from the Late Devonian of Southwest Ireland, *Sedimentary Geology,* v. 85, pp. 375-386.

Sharma, R. J. (2013). Fluvial architecture and sequence stratigraphy of the Upper Williams Fork Formation, Plateau Creek Canyon, Piceance Basin, Colorado. *University of Colorado at Boulder*.

Stoner, S. B. (2010). Fluvial architecture and geometry of the Mungaroo Formation on the Rankin Trend of the Northwest Shelf of Australia. *The University of Texas at Arlington* (Master's Thesis).

Strum, S. (1985). Lithofacies and Depositional Environments of the Raton Formation (*Upper Cretaceous-Paleocene*) of Northeastern New Mexico.

Topper, R., Scott, K., & Watterson, N. (2011). Geologic model of the Purgatoire River watershed within the Raton Basin, Colorado. *Colorado Geological Survey*.

Tomanka, G. D. (2013). Morphology, Mechanisms, and Processes for the formation of a non-bifurcating fluvial-deltaic channel prograding into Grapevine Reservoir, Texas. *University of Texas at Arlington* (Master's Thesis).

Wood Jr, G. H., Johnson, R. B., & Dixon, G. H. (1957). Geology and Coal Resources of the Starkville-West on Area Las Animas County Colorado. *Geological Survey Bulletin,* v. 1051, pp. 1-76.

Woodward, L. A. (1983*). Geology and Hydrocarbon Potential of the Raton Basin, New Mexico.* United States (USA): Four Corners Geol. Soc.

Wolfe, J.A., and Upchurch. (1987). Leaf assemblages across the Cretaceous-Tertiary Boundary in Raton Basin, NM and CO**.** *Geology,* Vol. 84, pp. 5096-5100.

Wright K. (2005). Hay-Zama Lakes waterfowl staging and bald eagle nesting monitoring program. *Alberta Conservation Association*, pp. 1-21.

Vita

Personal Background   Sean Corbett Horne
                           Born August 19, 1993, Littleton, Colorado

Education   Masters of Science in Geology, 2018
                           Texas Christian University, Fort Worth, Texas

                           Bachelors of Science in Geology, 2016
                           Colorado State University, Fort Collins, Colorado

Experience   Geoscience Intern, Summer 2018
                           Whiting Petroleum, Denver, Colorado

                           Geoscience Intern, Summer 2016
                           Orion International Ltd., Golden, Colorado

Professional Associations American Association of Petroleum Geologists
                           Rocky Mountain Association of Geologists
                           Geological Society of America
                           Fort Worth Geological Society

Abstract

DEPOSITIONAL MODELING AND INTERACTION BETWEEN LITHOFACIES
ASSEMBLAGES OF CRETACEOUS-PALEOGENE STRATA OF THE RATON BASIN

by Sean Corbett Horne, M.S., 2018
Department of Geological Sciences
Texas Christian University

Dr. John Holbrook, Thesis Advisor, Professor of Geology

Dr. Richard Denne, Hunter Enis Chair of Petroleum Geology

Bo Henk, Adjunct Professor of Geology

The Raton Basin of Colorado and New Mexico is a Laramide foreland basin that has

been important to coal geology since its first identification as a coal resource in 1821, and as a

major Coal Bed Methane resource in the modern era. The interaction between the lithosomes

assemblages of strata within the Raton Basin is not fully understood. . This work utilizes well

log correlations, core descriptions, measured sections, and digital outcrop models to create

paleogeographic reconstructions of the Raton Formation depositional systems. The coaly, fine-

grained rocks of the lower and upper coal zones of the Upper Cretaceous to Paleogene Raton

Formation are indicative of deposition in a wet, channel-floodplain environment with

intermittent periods of basin scale lacustrine flooding. The coarser, sand-rich barren series of the

Raton Formation displays a fan shape geometry with abundant terminal splay and channel form

lithofacies suggesting deposition within the medial to distal zone of a distributive fluvial system.